

# 敦煌三危山地区晚泥盆世斜长花岗岩的发现及其地质意义<sup>\*</sup>

赵燕<sup>1</sup> 第五春荣<sup>1</sup> 朱涛<sup>2</sup> 王洪亮<sup>2</sup> 孙勇<sup>1</sup>

ZHAO Yan<sup>1</sup>, DIWU ChunRong<sup>1</sup>, ZHU Tao<sup>2</sup>, WANG HongLiang<sup>2</sup> and SUN Yong<sup>1</sup>

1. 大陆动力学国家重点实验室, 西北大学地质学系, 西安 710069

2. 中国地质调查局西安地质调查中心, 西安 710054

1. State Key Laboratory of Continental Dynamics, Department of Geology, Northwest University, Xi'an 710069, China

2. Xi'an Center of Geological Survey, CGS, Xi'an 710054, China

2014-09-05 收稿, 2014-12-17 改回

**Zhao Y, Diwu CR, Zhu T, Wang HL and Sun Y. 2015. Discovery of the Late Devonian plagiogranite in Sanweishan area, Dunhuang, Gansu Province and its geological implications. *Acta Petrologica Sinica*, 31(7):1855–1869**

**Abstract** Plagiogranites in Sanweishan area, Dunhuang, Gansu Province are investigated for the first time. The plagiogranites, composed predominantly of plagioclase (60% ~ 65%) and quartz (28% ~ 32%), occur as small veins or net-veins. Plagioclase, mainly dominated by oligoclase, belongs to albite-oligoclase set ( $Ab = 85 \sim 99$ ). Samples studied in this paper are characterized by high  $SiO_2$  (71.00% ~ 72.92%), high  $Na_2O$  and low  $K_2O$  ( $Na_2O/K_2O = 8.54 \sim 11.37$ ) contents, with relatively higher  $Mg^#$  values ranging from 47 to 64. The chondrite-normalized rare earth element (REE) patterns are characterized by extremely low REE contents with relatively horizontal patterns and positive Eu and Sr anomalies. Analyses on zircon Hf isotopic compositions yield positive  $\varepsilon_{Hf}(t)$  values varying from +3.1 to +6.4, implying that the plagiogranite belongs to M-type granite. Field geological features, petrology, geochemistry, together with zircon Hf isotope compositions suggest that the plagiogranite in Sanweishan area is oceanic plagiogranite and this plagiogranite, experienced the later fluid interaction, was formed by cumulating of plagioclase in tholeiitic magma, which was derived from depleted mantle. Analyses on the zircon grains yield weighted mean  $^{206}Pb/^{238}U$  ages of  $363 \pm 2$  Ma and  $365 \pm 3$  Ma for samples 21SWS and SWS05, respectively, indicating that the plagiogranite formed at the Late Devonian. Based on the regional geological features, previous studies and our new data, we propose that Dunhuang area has ever undergone the formation and subduction of ocean basin, and the ocean basin, having begun to develop at 360 ~ 370 Ma, possibly is the back-arc basin of the southern margin of the Palaeo-Asian ocean; along with development since the Neoproterozoic and close of the Palaeo-Asian ocean, the Dunhuang block was likely to be involved into a series of orogenic events, and finally became a part of Central Asian Orogenic Belt.

**Key words** Sanweishan; Dunhuang; Plagiogranite; Late Devonian; Central Asian Orogenic Belt

**摘要** 本文报道在敦煌三危山地区发现的斜长花岗岩。斜长花岗岩呈细小脉状、网脉状产出, 主要由斜长石(60% ~ 65%)和石英(28% ~ 32%)组成, 电子探针分析数据显示斜长石属于钠长石-更长石( $Ab = 85 \sim 99$ ), 主要为更长石。岩石样品具高硅( $SiO_2 = 71.00\% \sim 72.92\%$ )、极度富钠、贫钾( $Na_2O/K_2O = 8.54 \sim 11.37$ )的特征;  $Mg^#$ 较高, 介于47 ~ 64; 稀土元素含量极低, 球粒陨石标准化配分曲线呈近乎平坦型分布, 轻、重稀土元素均亏损, Eu、Sr正异常。锆石Hf同位素组成显示 $\varepsilon_{Hf}(t)$ 为正值, 主体介于+3.1 ~ +6.4之间, 表明该斜长花岗岩为M型花岗岩。野外地质特征、岩相学特征、地球化学组成和锆石Hf同位素分析均表明该区斜长花岗岩是由起源于亏损地幔源区的洋脊拉斑玄武质熔体中的斜长石堆晶形成的大洋斜长花岗岩, 属于蛇绿岩的端元组分, 该岩石形成以后经历了后期流体交代作用的改造。LA-ICP-MS锆石U-Pb定年结果显示样品21SWS和SWS05的 $^{206}Pb/^{238}U$ 加权平均年龄分别为 $363 \pm 2$  Ma和 $365 \pm 3$  Ma, 表明该斜长花岗岩形成于晚泥盆世。综合区域地质特征及已有研究成果, 提出敦煌地区经历了晚古生代洋盆扩张-俯冲过程, 360 ~ 370 Ma的洋盆扩张可能代表了古亚洲洋南

\* 本文受中国地质调查局项目(1212011121137)和西北大学大陆动力学国家重点实验室科技部专项联合资助。

第一作者简介: 赵燕, 女, 1989年生, 博士生, 矿物学、岩石学、矿床学专业, E-mail: zhaoyan9917@126.com

缘弧后盆地的扩张;伴随着新元古代开始古亚洲洋的扩张-闭合过程,敦煌地块很可能卷入到了一系列与古亚洲洋闭合相关的造山活动,最终构成了中亚造山带的一部分。

**关键词** 三危山;敦煌;斜长花岗岩;晚泥盆世;中亚造山带

**中图法分类号** P588. 121; P597. 3

斜长花岗岩的形成与蛇绿岩的形成和演化具有直接或间接的联系,对于解释区域大地构造演化具有重要意义。蛇绿岩从大洋中脊分离、运移、俯冲到仰冲就位整个过程都可能产生斜长花岗岩,斜长花岗岩既可以呈小规模浅色脉体作为蛇绿岩的组成部分产出,也可以规模较大的独立岩株形式出现(Searle and Malpas, 1980; Gerlach *et al.*, 1981; Pedersen and Malpas, 1984; Pearce, 1989; Flagler and Spray, 1991; Bebout and Barton, 1993; 汪相, 1993; Peters and Kamber, 1994; Jafri *et al.*, 1995; Amri *et al.*, 1996; Whitehead *et al.*, 2000; Scarrow *et al.*, 2001; 李武显和李献华, 2003; Li and Li, 2003; 简平等, 2003a, b; France *et al.*, 2010)。产于洋中脊的大洋斜长花岗岩作为蛇绿岩的组成部分,其形成年龄代表洋壳的形成年龄,对于理解区域构造演化格局具有重要意义(Coleman and Peterman, 1975; Coleman and Donato, 1979; Gerlach *et al.*, 1981; 汪相, 1993; Amri *et al.*, 1996; 李武显和李献华, 2003; 张旗等, 2008)。

敦煌地块被认为是稳定克拉通前寒武纪变质基底的组成部分,由出露于塔里木东南缘阿尔金北部-敦煌地区的米兰杂岩和敦煌杂岩组成(梅华林等, 1997; 许志琴等, 1999; Lu *et al.*, 2008; 张建新等, 2011; 孟繁聪等, 2011; 辛后田等, 2013)。米兰杂岩由TTG质片麻岩、紫苏花岗片麻岩、基性麻粒岩、斜长角闪岩、石榴斜长角闪岩、黑云角闪斜长片麻岩、大理岩以及各类后期的侵入体等组成,岩石变质程度可达高角闪岩-麻粒岩相(孙勇等, 1992; Lu *et al.*, 2008; 刘永顺等, 2009),敦煌杂岩由TTG质片麻岩和变质程度达高角闪岩相的变质表壳岩组成(梅华林等, 1997; Lu *et al.*, 2008)。

中亚造山带(CAOB)是世界上最大的增生型造山带之一(Şengör *et al.*, 1993; Jahn *et al.*, 2000; Kovalenko *et al.*, 2004; Windley *et al.*, 2001, 2007; Kröner *et al.*, 2008; Xiao *et al.*, 2010, 2013; Xiao and Santosh, 2014),北接西伯利亚克拉通,西延至乌拉尔山,南部与塔里木地块-华北地块相接(图1a)。塔里木地块-敦煌地块以北的天山造山带和北山造山带(图1b)均属于中亚造山带的重要组成部分。已有研究表明,阿拉善地块北缘(郑荣国等, 2013; Zheng *et al.*, 2014)和塔里木地块北缘(Ge *et al.*, 2012)均受到了古亚洲洋古生代俯冲-碰撞造山作用的影响。敦煌地块处于一个特殊的大地构造位置,北接北山造山带,西北部接天山造山带,西南部接阿尔金造山带,东南部以阿尔金断裂与祁连造山带相隔(图1b)。近年来的研究主要集中于其前寒武纪基底的形成、演化(梅华林等, 1997, 1998; 赵燕等, 2013; Zhang *et al.*, 2012, 2013; Zong *et al.*, 2013)和早古生代构造热事件(张志诚等, 2009; Zong *et al.*, 2012; He *et al.*, 2014),对于

该地区晚古生代构造热事件鲜有报道,仅朱涛等(2014)对敦煌西南部青石沟地区的埃达克岩进行了研究,LA-ICP-MS锆石U-Pb定年结果显示该埃达克岩形成于早-中石炭世(335 Ma)。然而,敦煌地区晚古生代其他时代构造热事件及其与上述埃达克岩在时间、空间上的联系,以及敦煌地块与中亚造山带的关系等内容未有报道。

本文针对三危山地区出露的斜长花岗岩进行了详细的野外地质调查及岩相学、岩石地球化学分析,锆石U-Pb定年和Lu-Hf同位素组成测定,确定了其形成时代,初步探讨了岩石成因、岩浆源区性质和区域地质意义,以期为敦煌地块晚古生代构造热事件和构造演化研究提供依据。

## 1 地质概况和样品特征

典型的敦煌杂岩出露于敦煌三危山、旱峡、党河水库、东巴兔山、石包城、红柳峡河等地区,在北山地区少量出露(图1c)。已有研究表明敦煌地块至少经历了~3.06 Ga(赵燕等, 2015)、2.7~2.6 Ga(梅华林等, 1998; Zong *et al.*, 2013)、~2.5 Ga(赵燕等, 2013; Zhang *et al.*, 2013)和1.86~1.82 Ga(Zhang *et al.*, 2012, 2013; 赵燕等, 2013)四期前寒武纪构造热事件,且遭受了早古生代构造热事件的改造(张志诚等, 2009; 孟繁聪等, 2011; Zong *et al.*, 2012; He *et al.*, 2014)。朱涛等(2014)报道了阿克塞地区335 Ma的埃达克岩。三危山地区形成于136~99 Ma的基性岩墙群指示敦煌地区该时期处于伸展构造环境(冯志硕等, 2010)。由此可见,敦煌地区经历了多期构造活动和岩浆作用的改造,其构造演化具有复杂性、长期性和多阶段性演化特点。

本文所研究的斜长花岗岩出露于敦煌市东南大约25 km处的三危山地区(图1c),该地区断裂构造发育,主断裂沿NE-SW方向展布(图2),与阿尔金断裂的走向一致,主要出露云母石英片岩、黑云斜长片麻岩、斜长角闪岩、大理岩、花岗岩、花岗伟晶岩脉、斜长花岗斑岩脉和基性岩脉(图2)。1:20万敦煌幅地质图将云母石英片岩、黑云斜长片麻岩、斜长角闪岩和大理岩划分为前震旦纪敦煌杂岩的组成部分,并认为花岗岩、花岗伟晶岩脉、斜长花岗斑岩脉和基性岩墙侵入于敦煌杂岩中(甘肃省地质局区测二队, 1975)。根据野外地质特征和已有研究成果,基性岩墙的形成代表了该区最晚期的岩浆活动(冯志硕等, 2010),但是关于花岗岩、花岗伟晶岩及斜长花岗岩的形成序列仍需进一步研究,且在野外并未发现斜长花岗岩与周围的斜长角闪岩(图3c)呈热侵入接触关系的证据。

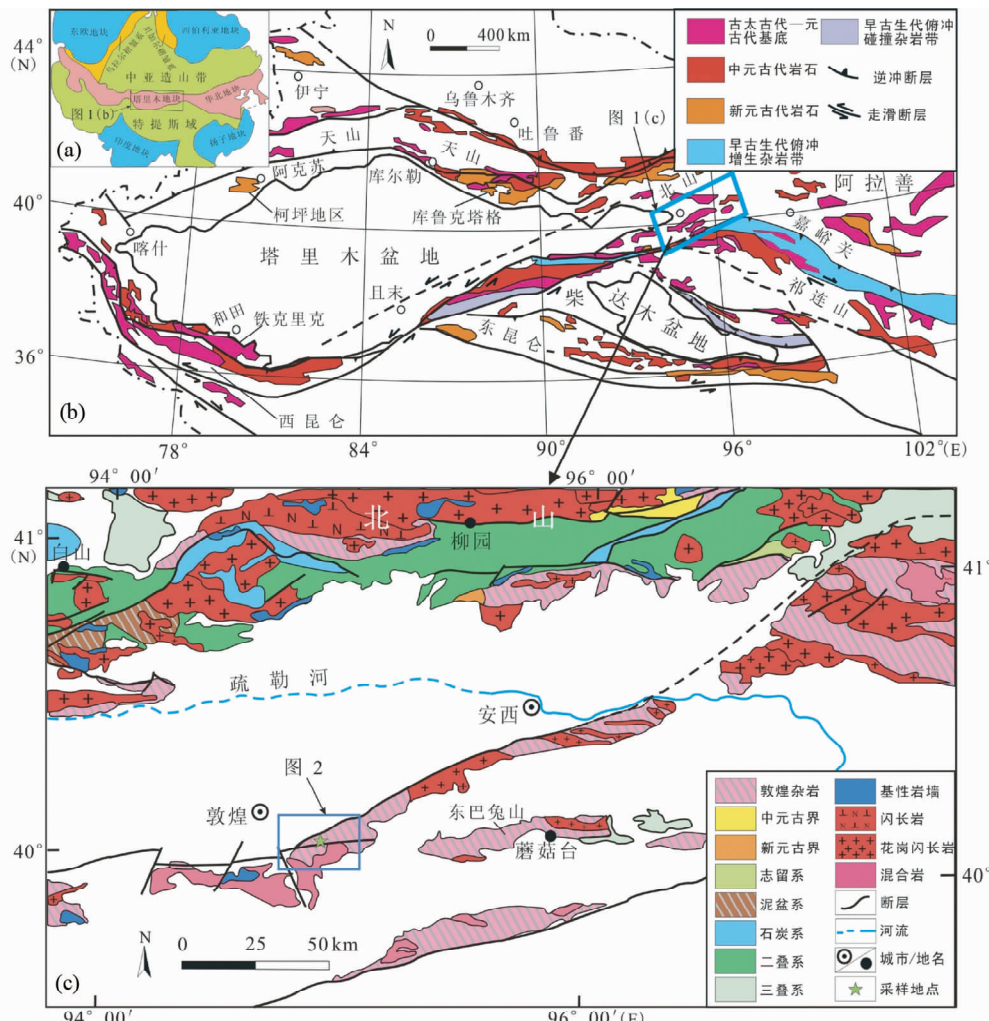


图1 中亚造山带构造简图(a, 据Sengör and Natal' in, 1993)、敦煌地块及邻区构造简图(b, 据Lu et al., 2008)与敦煌杂岩地质简图(c, 据中国地质调查局, 2004<sup>①</sup>)

Fig. 1 Tectonic sketch map of the Central Asian Orogenic Belt (a, after Sengör and Natal' in, 1993), simplified geological map of Dunhuang block (b, after Lu et al., 2008) and adjacent areas and simplified geological map of Dunhuang complex (c)

文中分析了样品21SWS和样品SWS05。野外地质观察表明样品呈小的脉状、网脉状产出,浅灰白色,块状构造(图3a, c),中粗粒结构,受区域断裂构造影响局部显示碎斑状结构(图3b, d)。样品主要由斜长石(60%~65%)和石英(28%~32%)组成,含少量白云母(<3%)和极少量绿帘石,副矿物有锆石、磷灰石等。斜长石呈他形-半自形板柱状,粒径1~6 mm不等,表面多绢云母化,对斜长石进行电子探针分析,计算出端元组分An=0~14,主体介于6~14,Ab=85~99,Or=0.02~2.34,属于钠长石-更长石系列,以更长石为主(表1)。石英表面干净,分为两类,一类呈细粒状充填于斜长石间隙,粒径<0.3 mm,具有波状消光现象,这类石英可能代表了岩浆期后的热液充填作用或者由区域断裂构造导致;另一类石英粒度较大(1.5~3 mm),与斜长石交

互生长,二者接触界限截然,这类石英是岩浆作用过程中形成的(图3b, d)。白云母呈不规则鳞片状沿斜长石裂隙和矿物间隙生长,指示其形成于晚期;绿帘石呈细粒状集合体分布于斜长石裂隙或边界(图3b, d)。

## 2 分析方法

除锆石分选工作在河北省廊坊市区域地质研究所实验室完成以外,全岩主、微量元素分析,锆石前期处理工作、锆石U-Pb定年和Lu-Hf同位素测定均在西北大学大陆动力学国家重点实验室完成。

全岩主量元素分析采用玻璃熔饼法在X荧光光谱仪

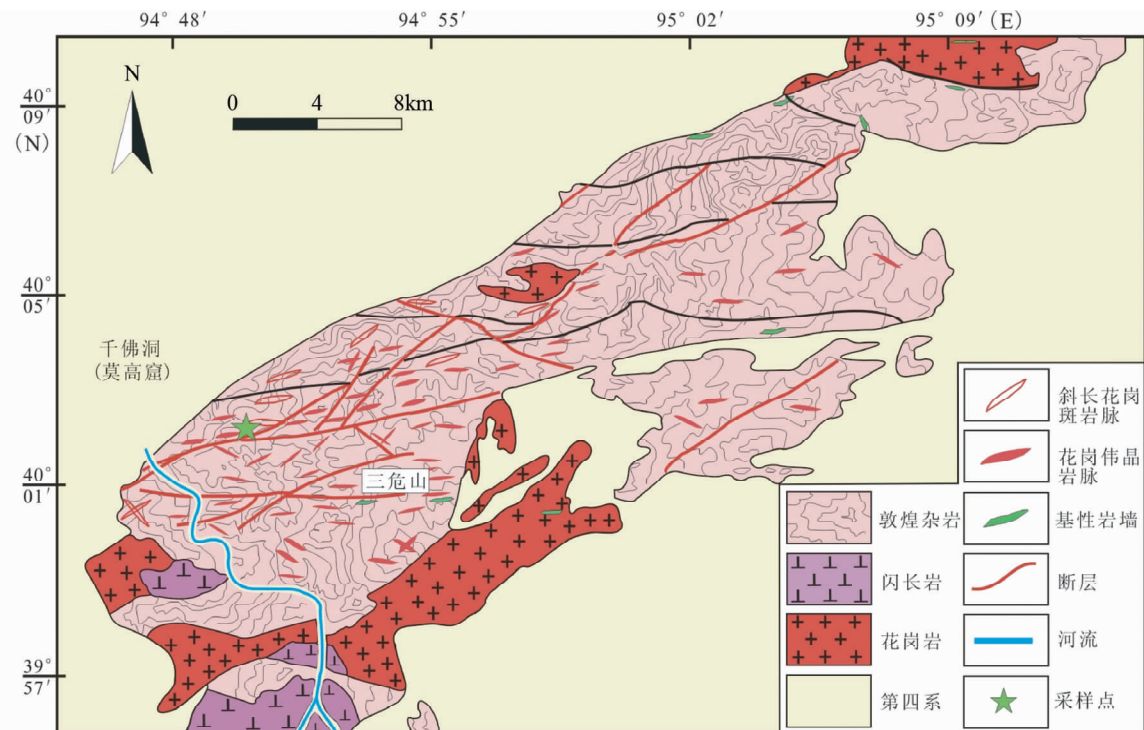


图2 敦煌三危山地区地质简图(据甘肃省地质局第一区域地质测量队, 1966<sup>①</sup>; 甘肃省地质局区测二队, 1975<sup>②</sup>; 甘肃省地质局地质力学区测队, 1976<sup>③</sup>)

Fig. 2 Simplified geological map of Sanweishan area

表1 敦煌三危山斜长花岗岩中代表性斜长石电子探针成分(wt%)

Table 1 Representative analyses of plagioclase in plagiogranite from Sanweishan area, Dunhuang (wt%)

测点号	21SWS	21SWS	21SWS	21SWS	21SWS	21SWS	21SWS	SWS05							
	-1	-2	-3	-4	-5	-6	-7	-1	-2	-3	-4	-5	-6	-7	-8
SiO <sub>2</sub>	68.20	66.88	64.32	66.62	67.15	65.18	64.57	65.99	65.48	66.11	65.43	65.51	69.40	65.81	65.52
TiO <sub>2</sub>	0.02	0.00	0.00	0.03	0.06	0.04	0.00	0.03	0.02	0.03	0.00	0.00	0.00	0.00	0.01
Al <sub>2</sub> O <sub>3</sub>	19.58	20.32	20.99	20.39	20.23	21.47	21.26	21.33	21.30	21.15	21.44	21.49	18.99	21.55	21.25
FeO	0.01	0.00	0.00	0.01	0.01	0.04	0.02	0.02	0.00	0.07	0.03	0.01	0.02	0.00	0.00
MgO	0.00	0.01	0.02	0.00	0.00	0.02	0.00	0.01	0.00	0.00	0.00	0.00	0.01	0.00	0.00
MnO	0.02	0.00	0.00	0.00	0.00	0.00	0.04	0.00	0.00	0.00	0.01	0.03	0.00	0.00	0.00
CaO	0.65	1.35	2.85	1.91	1.60	2.61	2.55	2.74	2.64	1.93	2.93	3.01	0.00	2.51	2.75
Na <sub>2</sub> O	11.55	11.23	10.12	10.95	11.15	9.89	10.15	10.13	10.15	10.72	10.20	10.43	12.19	10.08	10.33
K <sub>2</sub> O	0.13	0.08	0.20	0.09	0.05	0.41	0.31	0.22	0.20	0.17	0.14	0.12	0.00	0.14	0.24
SrO	0.40	0.30	0.38	0.32	0.29	0.37	0.39	0.43	0.33	0.43	0.32	0.29	0.24	0.39	0.41
Total	100.59	100.18	99.35	100.33	100.59	100.02	99.29	100.93	100.13	100.63	100.51	100.90	100.87	100.51	100.55
An	2.97	6.18	13.31	8.73	7.34	12.41	12.00	12.85	12.41	8.96	13.58	13.66	0.00	12.01	12.67
Ab	96.30	93.36	85.56	90.75	92.40	85.25	86.28	85.94	86.50	90.09	85.62	85.68	99.98	87.17	86.00
Or	0.72	0.46	1.13	0.51	0.27	2.34	1.72	1.21	1.09	0.95	0.80	0.66	0.02	0.82	1.33

(XRF, Rigaku RIX2100)上测定, 分析精度优于2%; 全岩微量元素和稀土元素测试在电感耦合等离子质谱(ICP-MS)仪上测

定, 样品测试中以AGV-2、BHVO-2、BCR-2、GSP-1为标样监控, 分析误差小于5%~10%。

① 甘肃省地质局第一区域地质测量队. 1966. 1:20万安西幅地质图(K-46-38)

② 甘肃省地质局区测二队. 1975. 1:20万敦煌幅地质图(K-46-35)

③ 甘肃省地质局地质力学区测队. 1976. 1:20万肃北幅地质图(J-46-5)

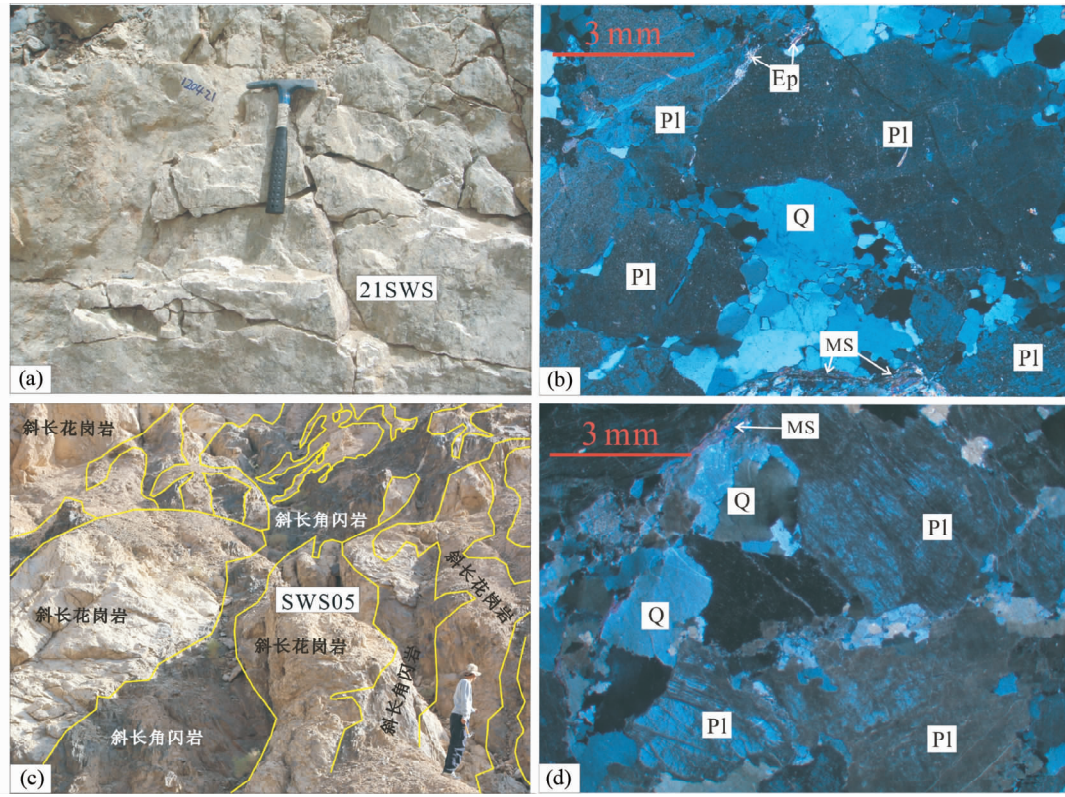


图3 敦煌三危山斜长花岗岩野外特征(a、c)及显微照片(b、d)

Pl-斜长石; Q-石英; MS-白云母; Ep-绿帘石

Fig. 3 The field geological photographs (a, c) and microstructures (b, d) of plagiogranite from Sanweishan area, Dunhuang  
Pl-plagioclase; Q-quartz; MS-muscovite; Ep-Epidote

锆石 U-Pb 年龄和微量元素分析测定是在连接 193nm 深紫外 ArF 激光器 (Geolas 2005) 的 Agilent 7700 型 ICP-MS 上进行的, 激光束斑直径为 32 $\mu\text{m}$ , 采用单点剥蚀方式, 激光剥蚀样品的深度为 20~30 $\mu\text{m}$ 。数据处理采用 Glitter (Ver4.0) 程序, 年龄计算以标准锆石 91500 为外标进行同位素比值分馏校正, 元素浓度计算采用 NIST 610 做外标,  $^{29}\text{Si}$  为内标, 样品的谐和图、加权平均年龄计算及图件绘制采用 Isoplot 软件 (Ludwig, 2003)。

锆石原位 Lu-Hf 同位素测定在配备了 Geolas 2500 激光剥蚀系统的 Nu Plasma HR 多接收电感耦合等离子体质谱仪 (MC-ICP-MS) 上完成, 激光剥蚀脉冲频率为 10Hz, 激光束斑直径为 44 $\mu\text{m}$ , 剥蚀时间约 50s。用  $^{175}\text{Lu}/^{176}\text{Lu} = 0.02655$  和  $^{176}\text{Yb}/^{172}\text{Yb} = 0.5886$  (Chu *et al.*, 2002) 进行校正,  $\varepsilon_{\text{Hf}}(t)$  计算采用  $^{176}\text{Lu}$  衰变常数为  $1.867 \times 10^{-11}$  a (Albarède *et al.*, 2006), 球粒陨石的  $^{176}\text{Hf}/^{177}\text{Hf}$  比值为 0.282785,  $^{176}\text{Lu}/^{177}\text{Hf}$  的比值为 0.0336 (Bouvier *et al.*, 2008), Hf 单阶段模式年龄  $t_{\text{DM}}$  的计算以现今的亏损地幔值为参考, 其  $^{176}\text{Hf}/^{177}\text{Hf} = 0.28325$ ,  $^{176}\text{Lu}/^{177}\text{Hf} = 0.0384$  (Griffin *et al.*, 2000)。两阶段 Hf 模式年龄 ( $t_{\text{DM2}}$ ) 计算时, 平均地壳的值采用  $^{176}\text{Lu}/^{177}\text{Hf} = 0.015$  (Rudnick and Gao, 2003)。

### 3 分析结果

#### 3.1 地球化学特征

敦煌三危山斜长花岗岩样品的主、微量元素分析结果见表 2。

主要元素分析结果显示, 样品具有高  $\text{SiO}_2$ 、极度富 Na 贫 K、低 Ti 高  $\text{Mg}^{\#}$  值等典型的斜长花岗岩特征,  $\text{SiO}_2 = 71.00\% \sim 72.92\%$ ,  $\text{Al}_2\text{O}_3 = 15.84\% \sim 16.13\%$ ,  $\text{Na}_2\text{O} = 6.35\% \sim 6.96\%$ ,  $\text{K}_2\text{O} = 0.93\% \sim 1.13\%$ ,  $\text{Na}_2\text{O}/\text{K}_2\text{O} = 8.54 \sim 11.37$ ,  $\text{TiO}_2 = 0.01\% \sim 0.03\%$ ,  $\text{Mg}^{\#} = 47.3 \sim 64.1$ 。里特曼指数  $\delta = 1.87 \sim 2.23$ , 为钙碱性系列。A/CNK = 0.92 ~ 1.06, 属于准铝质-弱过铝质岩石。在标准矿物计算结果中, 石英为 22.22% ~ 28.14%, 钠长石、钾长石和钙长石分别为 54.71% ~ 60.10%, 5.61% ~ 6.80%, 9.13% ~ 10.23%。

岩石样品中稀土含量极低,  $\Sigma \text{REE} = 0.69 \times 10^{-6} \sim 1.12 \times 10^{-6}$ ; 轻重稀土分馏不明显,  $(\text{La}/\text{Yb})_N = 1.05 \sim 2.99$ ; 轻稀土较重稀土轻微富集,  $\Sigma \text{LREE}/\Sigma \text{HREE} = 1.77 \times 10^{-6} \sim 3.41 \times 10^{-6}$ ; 稀土元素球粒陨石标准化配分曲线显示近乎平坦型分布 (图 4a), 明显 Eu 正异常,  $\delta \text{Eu} = 4.77 \sim 7.10$ 。明显 Eu 正异常暗示了斜长石的堆晶作用。微量元素原始地幔模

表 2 敦煌三危山斜长花岗岩主量元素(wt%)、微量元素( $\times 10^{-6}$ )分析结果Table 2 Major (wt%) and trace element ( $\times 10^{-6}$ ) for plagiogranite from Sanweishan area, Dunhuang

样品号	SWS05	21SWSK	21SWSK -1	样品号	SWS05	21SWSK	21SWSK -1	样品号	SWS05	21SWSK	21SWSK -1
SiO <sub>2</sub>	72.92	71.07	71.00	Cu	0.44	1.68	1.34	Ti	180	59.9	59.9
TiO <sub>2</sub>	0.03	0.01	0.01	Zn	6.51	3.26	3.12	Yb	0.055	0.060	0.060
Al <sub>2</sub> O <sub>3</sub>	15.84	16.13	15.98	Ga	12.3	11.7	11.9	Lu	0.0096	0.010	0.010
Fe <sub>2</sub> O <sub>3</sub> <sup>T</sup>	0.26	0.18	0.17	Ge	0.76	0.59	0.56	Hf	0.64	0.31	0.36
MnO	0.01	0.01	0.01	Rb	32.2	20.9	22.7	Ta	0.19	0.078	0.078
MgO	0.10	0.11	0.13	Sr	543	650	650	Pb	21.9	17.2	16.8
CaO	1.82	2.75	2.66	Y	0.50	0.51	0.48	Th	0.043	0.046	0.016
Na <sub>2</sub> O	6.35	6.96	6.92	Zr	18.4	9.53	11.2	U	0.16	0.041	0.044
K <sub>2</sub> O	1.13	0.93	0.98	Nb	0.96	0.20	0.20	Nb/Ta	5.03	2.55	2.51
P <sub>2</sub> O <sub>5</sub>	0.01	0.01	0.01	Cs	0.81	0.63	0.65	Zr/Hf	28.91	31.23	30.79
LOI	1.71	2.10	2.13	Ba	172	180	193	$\Sigma$ LREE	0.87	0.76	0.44
Total	100.18	100.26	100.00	La	0.23	0.16	0.088	$\Sigma$ HREE	0.25	0.27	0.25
Na <sub>2</sub> O/K <sub>2</sub> O	8.54	11.37	10.73	Ce	0.31	0.29	0.14	$\Sigma$ REE	1.12	1.03	0.69
Mg <sup>#</sup>	47.3	58.7	64.1	Pr	0.041	0.035	0.019	$\delta$ Eu	4.77	5.54	7.10
A/CNK	1.06	0.92	0.92	Nd	0.17	0.14	0.081	(La/Yb) <sub>N</sub>	2.99	1.93	1.05
$\delta$	1.87	2.22	2.23	Sm	0.041	0.040	0.030	石英(Q)	28.14	22.22	22.40
Li	6.64	4.81	5.34	Eu	0.077	0.087	0.087	刚玉(C)	0.90	0.00	0.00
Be	1.49	1.35	1.37	Gd	0.059	0.059	0.047	钾长石(Or)	6.80	5.61	5.93
Sc	0.47	0.36	0.34	Tb	0.0095	0.0091	0.0077	钠长石(Ab)	54.71	60.10	59.93
V	2.60	1.17	1.07	Dy	0.060	0.059	0.057	钙长石(An)	9.13	10.23	9.87
Cr	4.01	4.51	3.51	Ho	0.013	0.014	0.013	钛铁矿(II)	0.02	0.02	0.02
Co	37.8	59.1	60.2	Er	0.042	0.048	0.047	磷灰石(Ap)	0.02	0.02	0.02
Ni	3.06	2.52	2.03	Tm	0.0074	0.0096	0.0086				

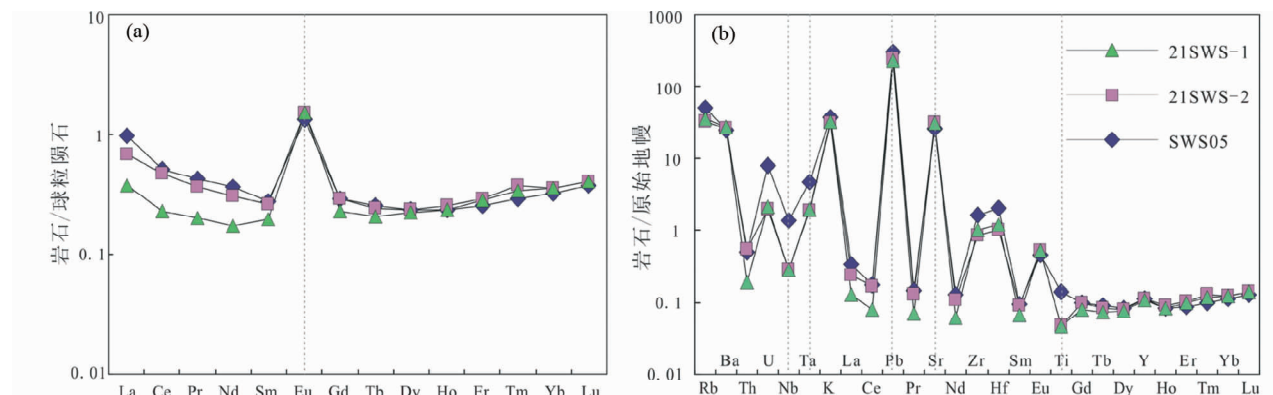


图 4 敦煌三危山斜长花岗岩球粒陨石标准化稀土元素配分图(a)和原始地幔标准化微量元素蛛网图(b)(标准化值据 Sun and McDonough, 1989)

Fig. 4 Chondrite-normalized REE patterns (a) and primitive mantle-normalized spidergrams (b) for plagiogranite from Sanweishan area, Dunhuang (normalization values after Sun and McDonough, 1989)

网图显示,大离子亲石元素(LILE) Rb、Ba、K、Pb、Sr等选择性富集,高场强元素(HFSE) Nb、Ta、Ti等相对亏损,而Zr、Hf相对富集(图4b)。岩石具有极低的Nb/Ta和Zr/Hf比值(Nb/Ta=2~5; Zr/Hf=28~32; 表2)。

### 3.2 锆石 U-Pb 年龄及稀土元素特征

三危山斜长花岗岩中的锆石呈淡黄色,自形长柱状,长

轴约60~100μm,短轴约30~50μm,长宽比2:1~3:1之间(图5)。锆石阴极发光图像显示特征的岩浆振荡环带结构。锆石具有低的Th含量和高的U含量,样品21SWS的Th含量为 $5.98 \times 10^{-6}$ ~ $68.5 \times 10^{-6}$ ,U含量为 $447 \times 10^{-6}$ ~ $2131 \times 10^{-6}$ ,Th/U比值为0.01~0.03;样品SWS05的Th含量为 $2.70 \times 10^{-6}$ ~ $79.3 \times 10^{-6}$ ,U含量为 $232 \times 10^{-6}$ ~ $1503 \times 10^{-6}$ ,Th/U比值为0.01~0.05(表3)。虽然通常认为岩

表3 敦煌三危山地区斜长花岗岩 LA-ICP-MS 锆石 U-Pb 定年结果

Table 3 LA-ICP-MS zircon U-Pb data for plagiogranite from Sanweishan area, Dunhuang

测点号	Th	U	Pb*	同位素比值						年龄(Ma)						
	( $\times 10^{-6}$ )	Th/U	$\frac{^{207}\text{Pb}}{^{206}\text{Pb}}$	1 $\sigma$	$\frac{^{207}\text{Pb}}{^{235}\text{U}}$	1 $\sigma$	$\frac{^{206}\text{Pb}}{^{238}\text{U}}$	1 $\sigma$	$\frac{^{207}\text{Pb}}{^{206}\text{Pb}}$	1 $\sigma$	$\frac{^{207}\text{Pb}}{^{235}\text{U}}$	1 $\sigma$	$\frac{^{206}\text{Pb}}{^{238}\text{U}}$	1 $\sigma$		
<b>21SWS</b>																
1	28.4	1040	64.9	0.03	0.06231	0.00129	0.49585	0.00987	0.05769	0.0006	684.9	43.6	408.9	6.7	361.6	3.6
2	11.2	590	36.0	0.02	0.05890	0.00175	0.47018	0.01351	0.05787	0.00067	563.5	63.3	391.3	9.3	362.7	4.1
3	10.3	635	38.0	0.02	0.05572	0.0012	0.44261	0.00918	0.05760	0.00059	440.7	46.8	372.1	6.5	361.0	3.6
4	15.6	910	55.4	0.02	0.05552	0.00116	0.44760	0.00899	0.05845	0.00059	432.8	45.5	375.6	6.3	366.2	3.6
5	23.9	866	52.9	0.03	0.05920	0.00108	0.47070	0.00818	0.05764	0.00056	574.6	39.1	391.7	5.7	361.3	3.4
6	68.5	2131	129	0.03	0.05408	0.00072	0.43680	0.00546	0.05856	0.00054	374.4	30.0	368.0	3.9	366.9	3.3
7	65.9	2025	123	0.03	0.05532	0.00082	0.44171	0.00617	0.05790	0.00054	425.1	32.4	371.5	4.4	362.8	3.3
8	5.98	447	27.0	0.01	0.05374	0.0013	0.42999	0.01002	0.05803	0.00060	359.9	53.7	363.2	7.1	363.6	3.7
9	12.5	714	43.0	0.02	0.05568	0.00114	0.43978	0.00860	0.05728	0.00056	439.4	44.5	370.1	6.1	359.0	3.4
10	35.3	1038	64.8	0.03	0.05974	0.00104	0.47716	0.00786	0.05792	0.00055	594.1	37.3	396.1	5.4	363.0	3.4
<b>SWS05</b>																
1	10.3	406	24.2	0.03	0.05882	0.00177	0.47055	0.01382	0.05803	0.00070	560.5	64.3	391.6	9.5	363.6	4.2
2	8.67	501	30.0	0.02	0.05670	0.00233	0.4438	0.01779	0.05677	0.00078	479.3	89.0	372.9	12.5	356.0	4.8
3	32.0	1110	66.5	0.03	0.05703	0.00105	0.46119	0.00828	0.05866	0.00061	492.0	40.2	385.1	5.8	367.5	3.7
4	5.40	392	22.6	0.01	0.05479	0.00173	0.42919	0.01322	0.05681	0.00069	403.8	68.4	362.6	9.4	356.2	4.2
5	3.41	250	14.9	0.01	0.05732	0.00189	0.46465	0.01494	0.05879	0.00073	503.5	71.4	387.5	10.4	368.3	4.5
6	6.09	305	18.1	0.02	0.05761	0.00176	0.45591	0.01357	0.05739	0.00069	514.7	65.9	381.4	9.5	359.8	4.2
7	17.5	870	51.7	0.02	0.05610	0.00113	0.45658	0.00895	0.05902	0.00063	455.9	43.7	381.9	6.2	369.7	3.8
8	24.3	630	54.7	0.04	0.05578	0.00177	0.44497	0.01383	0.05785	0.00071	443.3	69.2	373.7	9.7	362.5	4.3
9	8.40	447	27.1	0.02	0.05468	0.00195	0.44103	0.01535	0.05849	0.00075	399.0	77.1	371.0	10.8	366.4	4.6
10	6.07	317	26.9	0.02	0.05506	0.00184	0.44816	0.01463	0.05902	0.00074	414.5	72.4	376.0	10.3	369.7	4.5
11	2.70	232	13.9	0.01	0.05855	0.00249	0.47179	0.01961	0.05842	0.00083	550.4	90.3	392.4	13.5	366.0	5.1
12	79.3	1503	87.9	0.05	0.05590	0.00088	0.44549	0.00692	0.05778	0.0006	448.0	34.4	374.1	4.9	362.1	3.7
13	8.35	494	29.6	0.02	0.05349	0.00159	0.43803	0.01272	0.05937	0.00071	349.5	65.6	368.9	9.0	371.8	4.3
14	30.7	1080	63.8	0.03	0.05732	0.00108	0.46477	0.00861	0.05878	0.00063	503.5	41.5	387.6	6.0	368.2	3.8
15	9.37	324	19.9	0.03	0.05457	0.00183	0.44226	0.01449	0.05875	0.00074	394.8	72.6	371.8	10.2	368.0	4.5

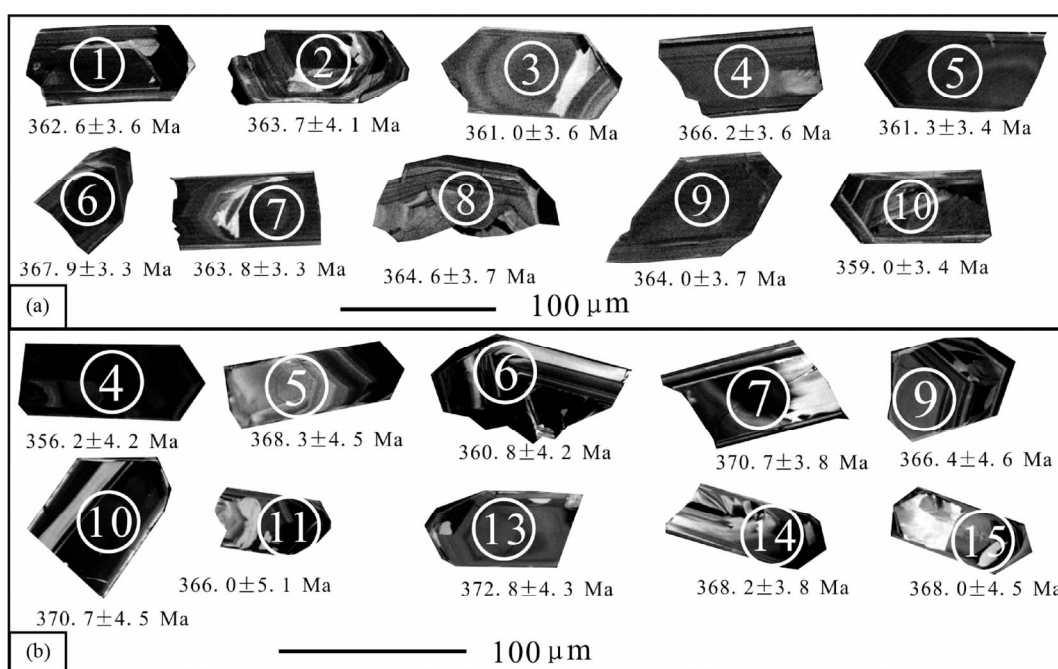


图5 敦煌三危山斜长花岗岩的锆石CL图像(a为样品21SWS; b为样品SWS05)

Fig. 5 CL images for zircons in plagiogranite from Sanweishan area, Dunhuang (a is Sample 21SWS; b is Sample SWS05)

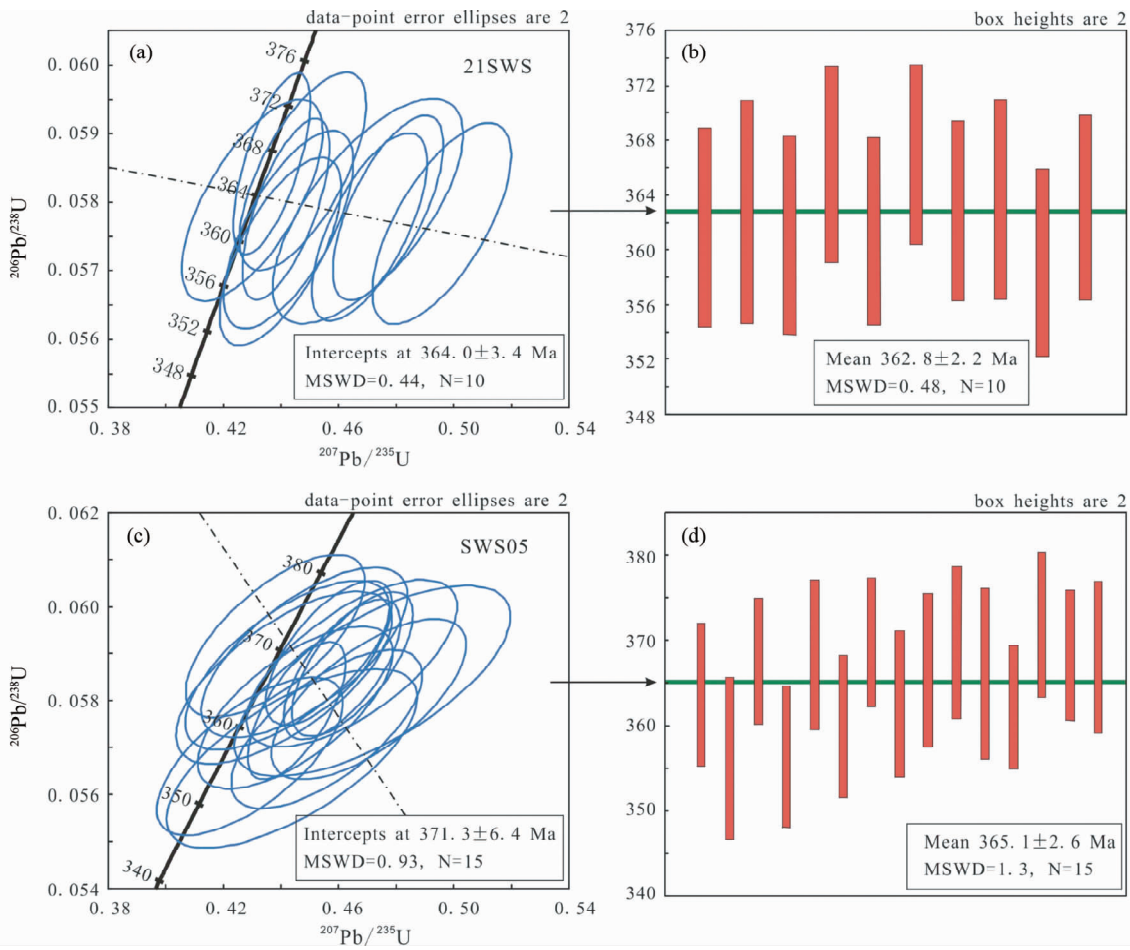


图 6 敦煌三危山斜长花岗岩锆石 U-Pb 年龄协和图(a、c)和 $^{206}\text{Pb}/^{238}\text{U}$ 加权平均年龄柱状图(b、d)

Fig. 6 U-Pb concordia diagrams (a, c) and weighted mean  $^{206}\text{Pb}/^{238}\text{U}$  ages (b, d) of zircons for plagiogranite

浆锆石的 Th/U 比值大于 0.4 (Rubatto and Gebauer, 2000; Belousova *et al.*, 2002),但是有些岩浆成因锆石的 Th/U 比值有时也会小于 0.1,比如澳大利亚新英格兰造山带 Weraera 地体 Upper Bingara 斜长花岗岩 (Aitchison and Ireland, 1995) 和金沙江娘九丁斜长花岗岩中都存在较多 Th/U 小于 0.1 的锆石 (简平等, 2003a),因此锆石 Th/U 比值不能用作判别锆石成因的唯一标志,依据锆石自形程度高、岩浆振荡环带明显的特征,确定该样品中的锆石为岩浆成因。

LA-ICP-MS 锆石 U-Pb 定年结果见表 3。样品 21SWS 中的 10 个锆石测点获得的 U-Pb 谱和年龄为  $364 \pm 3$  Ma (MSWD = 0.44) (图 6a),  $^{206}\text{Pb}/^{238}\text{U}$  加权平均年龄为  $363 \pm 2$  Ma (MSWD = 0.48) (图 6b)。样品 SWS05 中的 15 个锆石测点获得的 U-Pb 谱和年龄为  $371 \pm 6$  Ma (MSWD = 0.93) (图 6c),  $^{206}\text{Pb}/^{238}\text{U}$  加权平均年龄为  $365 \pm 3$  Ma (MSWD = 1.3) (图 6d)。上述两个加权平均年龄在误差范围内一致,该年龄代表了该斜长花岗岩的结晶年龄。

锆石微量元素分析结果见表 4。稀土元素球粒陨石标准化图解(图 7)显示,两个样品中的锆石均具有轻稀土亏损,

重稀土强烈富集且高度分异,明显 Ce 正异常和弱 Eu 负异常的特征(图 7a, b)。重稀土强烈富集且高度分异表明锆石结晶过程中没有石榴石的晶出(Sun *et al.*, 2002),弱 Eu 负异常与斜长石属于钠质斜长石吻合。

### 3.3 锆石 Lu-Hf 同位素

对进行了 LA-ICP-MS 锆石 U-Pb 定年分析的锆石测点进行 Lu-Hf 同位素测试,分析结果见表 5。除样品 21SWS 中测点 4 的  $^{176}\text{Lu}/^{177}\text{Hf}$  比值为 0.002064,样品 SWS05 中测点 7、8 的  $^{176}\text{Lu}/^{177}\text{Hf}$  比值分别为 0.002465 和 0.002757 以外,其余测点的  $^{176}\text{Lu}/^{177}\text{Hf}$  比值均小于 0.002,表明锆石形成后有极少量的放射性成因的 Hf 积累,测得的锆石 Hf 同位素组成基本可以代表锆石形成时体系的 Hf 同位素组成。样品 21SWS 和 SWS05 锆石 Hf 同位素的回时计算分别采用  $t = 363$  Ma 和  $t = 365$  Ma 作为斜长花岗岩的岩浆结晶年龄。

锆石 Lu-Hf 同位素分析结果显示,样品 21SWS 中 10 个锆石测点的 Hf 同位素组成较均一,  $^{176}\text{Hf}/^{177}\text{Hf}$  比值为 0.282680 ~ 0.282745,平均值为 0.282717,对应的  $\varepsilon_{\text{Hf}}(t)$  值为正值,介于 +4.0 ~ +6.2 (图 8),平均值为 +5.4,加权平均

表 4 敦煌三危山斜长花岗岩锆石微量元素含量( $\times 10^{-6}$ )Table 4 Trace element concentrations of zircons in plagiogranite from Sanweishan area, Dunhuang ( $\times 10^{-6}$ )

测点号	Ti	Sr	Y	Nb	La	Ce	Pr	Nd	Sm	Eu	Gd	Tb	Dy	Ho	Er	Tm	Yb	Lu	Hf	Ta
21SWS																				
1	7.13	1.44	1960	7.61	0.10	0.92	0.12	0.61	0.93	0.51	10.8	7.63	127	60.8	316	75.8	767	141	11088	0.70
2	5.39	0.72	1961	5.82	0.08	0.59	0.09	0.39	0.71	0.33	8.92	7.00	125	61.5	331	81.4	845	155	12975	0.53
3	3.64	0.79	2217	4.01	0.10	0.29	0.09	0.15	1.06	0.36	11.2	7.72	131	68.5	377	93.7	991	188	11787	0.41
4	3.69	1.07	2538	5.31	0.09	1.02	0.08	0.38	0.83	0.53	13.6	8.88	158	78.5	427	104	1109	204	12312	0.64
5	5.23	0.62	1886	5.82	0.10	0.70	0.11	0.26	0.96	0.52	9.94	6.67	120	59.3	311	74.6	777	146	12573	0.66
6	7.06	0.56	2835	11.1	0.13	1.41	0.09	0.29	1.31	0.72	20.1	12.4	200	91.4	447	99.9	982	169	12824	1.16
7	7.35	0.80	2520	10.5	0.12	1.66	0.09	0.61	1.41	0.85	20.0	11.7	185	82.5	401	89.5	868	152	12847	1.21
8	1.39	0.41	1385	3.30	0.10	0.31	0.10	0.13	0.74	0.28	5.61	4.06	78.0	41.6	242	61.3	663	132	13306	0.33
9	5.63	0.79	1964	9.91	0.06	0.70	0.10	0.29	0.75	0.41	7.97	5.86	114	61.5	342	84.2	894	169	12952	0.83
10	6.68	1.80	2745	11.7	0.08	2.42	0.18	1.50	1.88	1.09	18.9	11.1	190	87.3	443	103	1046	192	12924	1.21
SWS05																				
1	3.62	0.38	1535	1.93	0.00	0.32	0.01	0.04	0.33	0.21	6.22	4.95	90.7	47.8	269	67.9	733	154	12987	0.29
2	1.84	0.56	1803	2.59	0.05	0.75	0.03	0.48	0.72	0.45	7.66	5.17	104	54.4	320	81.4	880	182	14369	0.40
3	3.97	0.46	1244	6.27	0.00	0.64	0.03	0.21	0.58	0.35	7.99	4.91	82.7	39.5	208	50.0	506	96.4	14071	0.80
4	3.16	0.36	1589	1.70	0.00	0.25	0.03	0.06	0.18	0.31	7.57	5.03	95.3	50.1	279	69.2	732	149	13987	0.32
5	1.85	0.29	661	1.62	0.01	0.19	0.00	0.05	0.11	0.09	2.61	1.93	37.9	20.1	120	31.0	353	73.9	16001	0.37
6	2.13	0.28	1311	1.54	0.04	0.36	0.03	0.15	0.80	0.34	10.4	5.61	92.7	42.3	221	54.2	565	114	14120	0.26
7	3.72	0.59	2896	3.41	0.02	0.49	0.02	0.16	0.61	0.48	12.1	8.42	163	89.7	513	126	1325	223	15744	0.84
8	4.28	3.77	2108	4.41	0.01	0.22	0.01	0.06	0.13	0.24	2.68	8.25	131	64.3	358	90.4	981	202	15429	0.88
9	2.40	0.34	1423	3.06	0.00	0.25	0.00	0.06	0.24	0.19	7.06	4.99	88.7	44.2	250	63.0	665	135	14013	0.37
10	4.88	3.38	1020	1.42	0.06	0.79	0.07	0.47	1.02	0.51	13.5	8.15	168	92.8	535	137	1324	204	13469	0.77
11	2.32	0.25	775	1.71	0.03	0.13	0.02	0.14	0.20	0.11	3.06	2.25	43.7	23.2	138	36.5	397	81.4	15406	0.36
12	6.53	0.35	1634	8.09	0.04	1.19	0.02	0.31	1.31	0.51	12.5	7.23	115	53.2	265	60.3	596	112	13529	1.09
13	2.22	0.37	1135	2.02	0.01	0.31	0.00	0.04	0.50	0.08	5.26	3.44	66.7	35.2	206	53.0	584	121	19627	0.75
14	1.97	0.27	1183	7.71	0.05	0.57	0.00	0.17	0.53	0.23	6.42	4.09	74.7	38.1	207	50.8	530	102	14403	1.20
15	2.83	0.50	914	1.64	0.04	0.33	0.05	0.10	0.44	0.19	3.96	2.76	52.2	28.3	165	42.6	472	100	13762	0.41

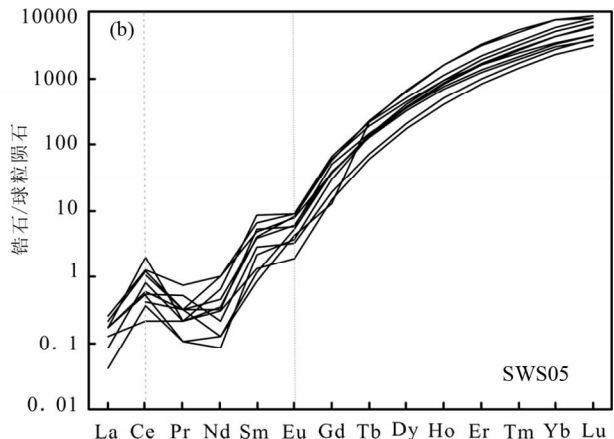
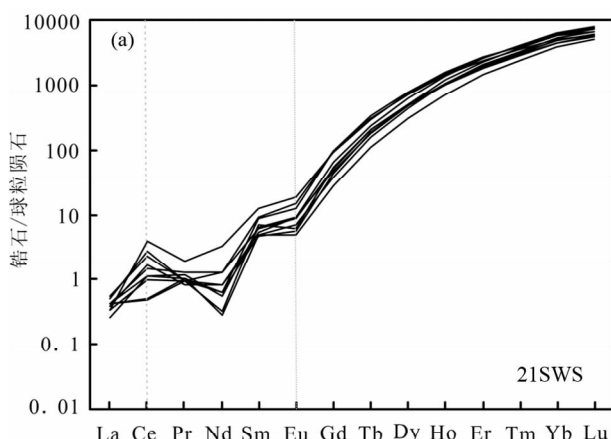


图 7 敦煌三危山斜长花岗岩锆石球粒陨石标准化微量元素图解(标准化值据 Sun and McDonough, 1989)

Fig. 7 Chondrite-normalized REE patterns of zircons in plagiogranite from Sanweishan area, Dunhuang ( normalization values after Sun and McDonough, 1989 )

值为  $5.5 \pm 0.5$ , 单阶段模式年龄为  $746 \sim 840$  Ma, 平均为 780 Ma, 两阶段模式年龄为  $965 \sim 1108$  Ma, 平均为 1019 Ma。对样品 SWS05 中 15 个锆石测点进行分析, 除点 10 具有较高的  $^{176}\text{Hf}/^{177}\text{Hf}$  比值 (0.282807), 对应的  $\varepsilon_{\text{Hf}}(t)$  值较高

(+8.8), 两阶段模式年龄较小 (806 Ma) 之外, 其余 14 个测点具有相对均一的 Hf 同位素组成,  $^{176}\text{Hf}/^{177}\text{Hf}$  比值介于 0.282660 ~ 0.282743, 平均值为 0.282710, 对应的  $\varepsilon_{\text{Hf}}(t)$  值为正值, 介于 +3.1 ~ +6.4 之间 (图 8), 平均值为 +5.1, 加权

表 5 敦煌三危山地区斜长花岗岩锆石 Lu-Hf 同位素测定结果

Table 5 Lu-Hf isotopic compositions of zircons for plagiogranite from Sanweishan area, Dunhuang

测点号	年龄 (Ma)	$\frac{^{176}\text{Yb}}{^{177}\text{Hf}}$	$\frac{^{176}\text{Lu}}{^{177}\text{Hf}}$	$\frac{^{176}\text{Hf}}{^{177}\text{Hf}}$	$\left(\frac{^{176}\text{Hf}}{^{177}\text{Hf}}\right)_i$	$2\sigma$	$\varepsilon_{\text{Hf}}(t)$	$2\sigma$	$t_{\text{DM1}}(\text{Ma})$	$t_{\text{DM2}}(\text{Ma})$	$f_{\text{Lu/Hf}}$
21SWS											
1		0.026771	0.001110	0.282711	0.282703	0.000013	5.3	0.5	780	1025	-0.97
2		0.041634	0.001564	0.282713	0.282702	0.000013	5.1	0.5	791	1035	-0.95
3		0.019294	0.000819	0.282680	0.282674	0.000023	4.3	0.8	816	1087	-0.98
4		0.048665	0.002064	0.282713	0.282699	0.000017	4.9	0.6	807	1049	-0.94
5	363	0.041281	0.001704	0.282741	0.282729	0.000011	6.1	0.4	756	976	-0.95
6		0.040540	0.001692	0.282745	0.282733	0.000017	6.2	0.6	750	967	-0.95
7		0.040064	0.001469	0.282742	0.282732	0.000014	6.2	0.5	746	965	-0.96
8		0.013405	0.000558	0.282716	0.282712	0.000018	5.7	0.6	757	997	-0.98
9		0.034009	0.001329	0.282732	0.282723	0.000011	5.9	0.4	757	985	-0.96
10		0.041001	0.001710	0.282682	0.282671	0.000017	4.0	0.6	840	1108	-0.95
SWS05											
1		0.039954	0.001036	0.282739	0.282732	0.000012	6.4	0.4	739	959	-0.97
2		0.051300	0.001496	0.282728	0.282718	0.000014	5.7	0.5	768	998	-0.95
3		0.039448	0.001116	0.282709	0.282702	0.000013	5.3	0.5	783	1028	-0.97
4		0.035344	0.001117	0.282677	0.282670	0.000011	4.1	0.4	828	1100	-0.97
5		0.033435	0.000992	0.282680	0.282673	0.000012	4.3	0.4	820	1089	-0.97
6		0.037796	0.001229	0.282716	0.282708	0.000013	5.5	0.5	776	1016	-0.96
7		0.084184	0.002465	0.282743	0.282726	0.000011	5.8	0.4	776	993	-0.93
8	365	0.065028	0.002006	0.282660	0.282646	0.000016	3.1	0.6	883	1167	-0.94
9		0.067543	0.001866	0.282726	0.282713	0.000015	5.5	0.5	782	1014	-0.94
10		0.038577	0.001064	0.282807	0.282800	0.000017	8.8	0.6	643	806	-0.97
11		0.092766	0.002757	0.282706	0.282688	0.000013	4.4	0.5	839	1085	-0.92
12		0.054329	0.001670	0.282734	0.282722	0.000017	5.9	0.6	765	990	-0.95
13		0.037563	0.001065	0.282739	0.282732	0.000013	6.3	0.5	739	959	-0.97
14		0.037584	0.001030	0.282690	0.282683	0.000015	4.6	0.5	808	1069	-0.97
15		0.035735	0.001066	0.282685	0.282678	0.000014	4.4	0.5	815	1080	-0.97

注:  $\varepsilon_{\text{Hf}}(t) = ((^{176}\text{Hf}/^{177}\text{Hf})_s - (^{176}\text{Lu}/^{177}\text{Hf})_s \times (e^{\lambda t} - 1)) / ((^{176}\text{Hf}/^{177}\text{Hf})_{\text{CHUR},0} - (^{176}\text{Lu}/^{177}\text{Hf})_{\text{CHUR}} \times (e^{\lambda t} - 1) - 1) \times 10000$ ;  $t_{\text{DM1}} = 1/\lambda \times \ln[1 + ((^{176}\text{Hf}/^{177}\text{Hf})_s - (^{176}\text{Hf}/^{177}\text{Hf})_{\text{DM}})/((^{176}\text{Lu}/^{177}\text{Hf})_s - (^{176}\text{Lu}/^{177}\text{Hf})_{\text{DM}})]$ ;  $t_{\text{DM2}} = t_{\text{DM1}} - (t_{\text{DM1}} - t)((f_{\text{CC}} - f_s)/(f_{\text{CC}} - f_{\text{DM}}))$ ;  $f_{\text{Lu/Hf}} = (^{176}\text{Lu}/^{177}\text{Hf})_s / (^{176}\text{Lu}/^{177}\text{Hf})_{\text{CHUR}} - 1$ ;  $f_{\text{cc}}$ -大陆地壳的  $f_{\text{Lu/Hf}}$ ;  $f_s$ -样品的  $f_{\text{Lu/Hf}}$ ;  $f_{\text{DM}}$ -亏损地幔的  $f_{\text{Lu/Hf}}$ ;  $t$ -样品形成时间;  $\lambda = 1.867 \times 10^{-11} \text{ year}^{-1}$

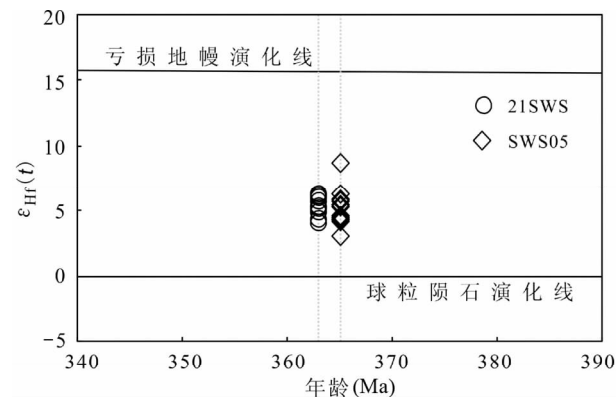


图 8 敦煌三危山地区斜长花岗岩锆石 Hf 同位素组成

Fig. 8 Zircon Hf isotopic compositions for plagiogranite from Sanweishan area, Dunhuang

平均值为  $5.1 \pm 0.5$ , 单阶段模式年龄为  $739 \sim 883 \text{ Ma}$ , 平均为794 Ma, 两阶段模式年龄为  $959 \sim 1167 \text{ Ma}$ , 平均为  $1039 \text{ Ma}$ 。

## 4 讨论

### 4.1 岩石类型及岩浆源区

野外地质特征显示,敦煌三危山地区的斜长花岗岩呈细小脉状,局部呈网脉状分布;岩相学方面,主要矿物组合为石英和斜长石,斜长石端元组分为  $\text{An} = 0 \sim 14$ ,  $\text{Ab} = 85 \sim 99$ ,  $\text{Or} = 0.02 \sim 2.34$ , 属于钠长石-更长石系列(表 1),且以更长石为主;岩石地球化学分析数据显示样品具有高  $\text{SiO}_2$  (71.00% ~ 72.92%)、极度富  $\text{Na}_2\text{O}$  (6.35% ~ 6.96%) 贫  $\text{K}_2\text{O}$  (0.93% ~ 1.13%) 的特征。这些特征均反映研究区斜长花岗岩与国内外一些典型的大洋斜长花岗岩相似(Coleman and Peterman, 1975; Amri et al., 1996; 张旗等, 2008; 李武显和李献华, 2003)。因此,综合该斜长花岗岩的野外产状、岩相

学特征、岩石地球化学成分特征,认为该斜长花岗岩属于大洋斜长花岗岩,属于蛇绿岩的组成部分。

锆石是一种非常稳定的副矿物,具有极度抗风化、高 Lu-Hf 同位素体系封闭温度、高 Hf 含量与低 Lu/Hf 比值等特点。锆石形成后,基本没有明显的放射性成因 Hf 积累,很少受到后期构造热事件的改造,在其形成以后即使在高级变质作用下也可以保存其形成时体系的 Hf 同位素组成,因此我们能够较为准确地获得锆石形成时的 Hf 同位素组成,这使得锆石 Hf 同位素研究成为目前探讨地壳演化和示踪岩石源区的重要工具(Patchett *et al.*, 1982; Amelin *et al.*, 1999, 2000; Griffin *et al.*, 2002; 吴福元等, 2007)。一般认为,具有低的<sup>176</sup>Hf/<sup>177</sup>Hf 比值以及  $\varepsilon_{\text{Hf}}(t)$  值的岩石往往指示地壳源区或者源区经过地壳物质的混染;而具有较高的<sup>176</sup>Hf/<sup>177</sup>Hf 比值以及  $\varepsilon_{\text{Hf}}(t)$  值的岩石直接来自亏损地幔或由起源于亏损地幔的新生壳源物质部分熔融形成(Corfu and Stott, 1993; Kinny and Maas, 2003)。对三危山斜长花岗岩进行锆石 Hf 同位素组成分析,样品 21SWS 中的锆石具有高的<sup>176</sup>Hf/<sup>177</sup>Hf (0.282671 ~ 0.282733) 和  $\varepsilon_{\text{Hf}}(t)$  值 (+4.0 ~ +6.2, 平均值为 +5.4), 样品 SWS05 中的锆石也具有高的<sup>176</sup>Hf/<sup>177</sup>Hf (0.282646 ~ 0.282800) 和  $\varepsilon_{\text{Hf}}(t)$  值 (+3.1 ~ +6.4, 平均值为 +5.1)。两个样品的锆石 Hf 同位素组成相对均一,且指示斜长花岗岩浆源自亏损地幔源区,为 M 型花岗岩。锆石两阶段和单阶段 Hf 模式年龄均远大于锆石的形成年龄,可能与岩浆从亏损地幔抽取后滞留时间较长有关。

同原始地幔相比,除大离子亲石元素 Rb、Ba、K、Sr 等比值远大于 1 外,其他微量元素,包括高场强元素 Nb、Ta、Th、U、Zr、Hf、Ti 和稀土元素 La、Ce、Sm 等的比值均小于 1 或接近于 1,亦显示了岩浆源自亏损地幔的性质,与锆石 Hf 同位素所指示的亏损地幔源区一致。

综上所述,敦煌三危山地区的斜长花岗岩为 M 型花岗岩,属于大洋斜长花岗岩,推测由拉张环境下洋盆扩张脊处源于亏损地幔源区的洋脊玄武质熔体中的斜长石堆晶形成,可近似代表洋壳的形成年龄。

#### 4.2 岩浆期后流体作用

岩相学特征显示,部分石英以细粒状充填于大颗粒的斜长石和石英间隙,且具有波状消光现象,这类石英的形成,一种原因与该区断裂构造发育,岩石形成后受区域动力变质作用有关;另一种原因可能与岩浆期后热液充填作用有关。鳞片状白云母和细粒绿帘石集合体沿斜长石裂隙或矿物边界分布,明显属于次生矿物,应该为热液蚀变的产物(丁兴等, 2012)。

从岩石地球化学方面来看,岩石具有极低的稀土元素含量,明显 Eu 正异常,不相容元素整体亏损,具有极低的 Nb/Ta 和 Zr/Hf 比值,远低于原始地幔的 Nb/Ta (17.2 ± 2.0) 和 Zr/Hf (36.27 ± 2.0) 比值,强烈富集 Rb、Ba、U、K、Pb 和 Sr 等活动性元素。这些特征与明显遭受流体分异的岩石特征类

似(Ding *et al.*, 2013),因此,岩石地球化学特征指示该斜长花岗岩遭受了流体作用的改造。

锆石 CL 图像显示(图 5),斜长花岗岩中的锆石具有弱的发光性,该特征与其 U 含量较高有关;大部分锆石的晶形和岩浆结晶环带都很完整,个别锆石局部遭受了显著的脱晶化作用。流体中一般富 U 贫 Th (Rowley *et al.*, 1997; Mojzsis and Harrison, 2002),因此,锆石极低的 Th/U 比值及其局部脱晶化特征暗示了流体作用对锆石的改造。

综合岩相学、地球化学和锆石特征来看,研究区斜长花岗岩形成后经历了后期流体交代作用。

#### 4.3 斜长花岗岩的形成时代及构造意义

对斜长花岗岩进行锆石 U-Pb 年龄测定,锆石颗粒呈自形长柱状,具典型的岩浆结晶振荡环带结构,具有岩浆型锆石的特征(图 5),因此,锆石是在岩浆结晶过程中形成的。锆石 U-Pb 年龄均较为谐和,表明岩浆期后的流体作用对锆石的影响并不大,即该过程中几乎没有放射性成因 Pb 丢失。LA-ICP-MS 锆石 U-Pb 定年结果显示,样品 21SWS 中的 10 个分析点具有一致的<sup>206</sup>Pb/<sup>238</sup>U 年龄值,<sup>206</sup>Pb/<sup>238</sup>U 加权平均年龄为  $362.8 \pm 2.2$ Ma (MSWD = 0.48);样品 SWS05 中的 15 个分析点的<sup>206</sup>Pb/<sup>238</sup>U 加权平均年龄为  $365.1 \pm 2.6$ Ma (MSWD = 1.3)。两个样品的<sup>206</sup>Pb/<sup>238</sup>U 加权平均年龄在误差范围内一致,说明该斜长花岗岩形成于 360 ~ 370Ma, 属于晚泥盆世,指示敦煌地区有泥盆世的岩浆侵位活动。该岩石为敦煌地区目前唯一发现的晚泥盆世岩浆活动记录,对于解释敦煌地块晚古生代动力学过程具有重要意义。

中亚造山带是世界上最大的增生型造山带之一(Sengör *et al.*, 1993; Jahn *et al.*, 2000; Kovalenko *et al.*, 2004; Windley *et al.*, 2001, 2007; Kröner *et al.*, 2008; Xiao *et al.*, 2010, 2013, 2014),被认为是由众多弧/弧后系统、蛇绿岩带及微陆块组成的(Jian *et al.*, 2008; Khain *et al.*, 2003; Kozakov *et al.*, 2001)。1000 ~ 700Ma 为古亚洲洋的打开阶段,形成了具有多岛分布的古亚洲洋;600 ~ 400Ma 为古亚洲洋强烈扩张期,伴随已形成洋壳向洋中微陆块的俯冲作用;400 ~ 200Ma 为古亚洲洋洋壳俯冲消减末期,并最终碰撞造山的阶段(陈岳龙等, 2013)。敦煌地块北接北山造山带,西北部为天山造山带,西接塔里木克拉通,东临阿拉善地块(图 1b)。天山造山带和北山造山带均属于中亚造山带的组成部分。天山地区广泛分布晚古生代(370 ~ 310Ma)的火山岩、侵入岩和超高压变质岩(张连昌等, 2004; 高俊等, 2006; 李锦铁等, 2006; Shi *et al.*, 2007; 陈刚等, 2010; 苏春乾等, 2009; 周涛发等, 2010; Long *et al.*, 2011; An *et al.*, 2013; Ma *et al.*, 2014; Xia *et al.*, 2014);北山地区高压/超高压变质岩形成于晚奥陶世-早志留世(Liu *et al.*, 2011; Qu *et al.*, 2011),指示北山地区的俯冲-碰撞事件发生在晚奥陶世-早志留世。阿拉善地块北缘(郑荣国等, 2013; Zheng *et al.*, 2014)和塔里木地块北缘(Ge *et al.*, 2012)亦受到了古亚洲

洋古生代俯冲-碰撞造山作用的影响。敦煌地块处于这样一个特殊的大地构造位置是否受到了古亚洲洋闭合事件的影响?

如前所述,研究区斜长花岗岩为M型花岗岩,属于大洋斜长花岗岩,由洋盆扩张脊处起源于亏损地幔源区的洋脊玄武质熔体中的斜长石堆晶形成,近似代表了洋壳形成年龄。朱涛等(2014)对甘肃阿克塞青石沟地区的埃达克岩进行研究,LA-ICP-MS锆石U-Pb年龄显示该埃达克岩形成于~335 Ma,岩石化学成分具有富钠贫钾( $\text{Na}_2\text{O}/\text{K}_2\text{O} = 2.4 \sim 2.9$ ),大离子亲石元素和轻稀土元素富集,Nb,Ta等高场强元素和重稀土强烈亏损的特征,很可能是俯冲板片在一定深度部分熔融的产物,代表了岛弧的形成。北山造山带的造山事件发生在晚奥陶世-早志留世,而天山造山带的主体碰撞造山事件为中-晚泥盆世,已有研究表明敦煌地区的造山事件可能发生在志留纪-早泥盆世(440~400 Ma; Zong *et al.*, 2012; He *et al.*, 2014)。因此,结合本文研究成果及区域地质特征,敦煌地区在晚泥盆世-早-中石炭世(370~330 Ma)经历了洋盆扩张-俯冲过程,且该洋盆可能代表了古亚洲洋南缘弧后盆地的扩张。

传统意义上,敦煌地块被认为是稳定克拉通前寒武纪变质基底的组成部分(梅华林等,1997;许志琴等,1999; Lu *et al.*, 2008; 张建新等,2011; 孟繁聪等,2011; 辛后田等,2013)。然而,已有研究表明,敦煌地区前寒武纪变质基底岩石只是零星的分布在敦煌地块中部(Zong *et al.*, 2013)及其南缘(梅华林等,1998; Zhang *et al.*, 2013; 赵燕等,2013),在整个敦煌地区持续记录了早古生代中-晚期及晚古生代早中期的构造-热事件,如蘑菇台地区430~440 Ma的基性高压麻粒岩(Zong *et al.*, 2012; He *et al.*, 2014)、党河水库地区440 Ma的TTG质岩石(张志诚等,2009)、三危山地区400~435 Ma斜长角闪岩(孟繁聪等,2011)以及敦煌西南部青石沟地区335 Ma埃达克岩(朱涛等,2014)等。因此,敦煌地块不是典型的稳定克拉通的组成部分,伴随着新元古代开始古亚洲洋的扩张-闭合过程,敦煌地块可能强烈卷入了一系列与古亚洲洋闭合相关的古生代造山活动,最终构成了中亚造山带的一部分。

## 5 结论

(1)野外地质、岩相学、岩石地球化学特征和锆石Hf同位素分析均表明三危山地区斜长花岗岩为大洋斜长花岗岩,形成于洋盆扩张过程,由起源于亏损地幔源区的洋脊拉斑玄武质熔体中的斜长石堆晶形成,属于蛇绿岩的组成部分;该岩石形成后遭受了后期流体交代作用的改造。

(2) LA-ICP-MS锆石U-Pb定年结果显示,敦煌三危山地区两个斜长花岗岩的 $^{206}\text{Pb}/^{238}\text{U}$ 加权平均年龄分别为363 Ma和365 Ma,表明该斜长花岗岩形成于晚泥盆世,该年龄结果代表了敦煌地块晚泥盆世洋盆扩张事件;综合区域地

质考虑,该期扩张很可能是古亚洲洋南缘弧后盆地的扩张。

(3)结合已有研究成果,提出伴随着新元古代开始古亚洲洋的扩张-闭合过程,敦煌地块很可能卷入到了一系列与古亚洲洋闭合相关的造山活动,最终构成了中亚造山带的一部分。

## References

- An F, Zhu YF, Wei SN and Lai SC. 2013. An Early Devonian to Early Carboniferous volcanic arc in North Tianshan, NW China: Geochronological and geochemical evidence from volcanic rocks. *Journal of Asian Earth Sciences*, 78: 100~113
- Aitchison JC and Ireland TR. 1995. Age profile of ophiolitic rocks across the Late Palaeozoic New England Orogen, New South Wales: Implications for tectonic models. *Australian Journal of Earth Sciences*, 42(1): 11~23
- Albarède F, Scherer EE, Blichert-Toft J, Rosing M, Simionovici A and Bizzarro M. 2006.  $\gamma$ -ray irradiation in the early Solar System and the conundrum of the  $^{176}\text{Lu}$  decay constant. *Geochimica et Cosmochimica Acta*, 70(5): 1261~1270
- Amri I, Benoit M and Ceuleneer G. 1996. Tectonic setting for the genesis of oceanic plagiogranites: Evidence from a paleo-spreading structure in the Oman ophiolite. *Earth and Planetary Science Letters*, 139(1~2): 177~194
- Amelin Y, Lee DC, Halliday AN and Pidgeon RT. 1999. Nature of the Earth's earliest crust from hafnium isotopes in single detrital zircon. *Nature*, 399(6733): 252~255
- Amelin Y, Lee DC and Halliday AN. 2000. Early-Middle Archaean crustal evolution deduced from Lu-Hf and U-Pb isotopic studies of single zircon grains. *Geochimica et Cosmochimica Acta*, 64(24): 4205~4225
- Bebout GE and Barton MD. 1993. Metasomatism during subduction: Products and possible paths in the Catalina schist, California. *Chemical Geology*, 108(1~4): 61~92
- Belousova EA, Griffin WL, O'Reilly SY and Fisher NI. 2002. Igneous zircon: Trace element composition as an indicator of source rock type. *Contributions to Mineralogy and Petrology*, 143(5): 602~622
- Bouvier A, Vervoort JD and Patchett PJ. 2008. The Lu-Hf and Sm-Nd isotopic composition of CHUR: Constraints from unequilibrated chondrites and implications for the bulk composition of terrestrial planets. *Earth and Planetary Science Letters*, 273(1~2): 48~57
- Chen G, Zhu ZX, Dong LH, Liu B, Ni XY and Zhao HL. 2010. Determination and geological significance of ocean island volcanic rocks of the Devonian-Early Carboniferous in Taxkorgan region, southern Tianshan of Xinjiang. *Xinjiang Geology*, 28(3): 236~241 (in Chinese with English abstract)
- Chen YL, Li DP, Liu CZ, Wang Z and Liu JB. 2013. The formation and evolution of Central Asian Orogenic Belt: Evidence from Zircon U-Pb ages and Hf isotopes, and whole-rock Nd isotopic compositions. *Acta Geologica Sinica*, 87(Suppl.): 374~376 (in Chinese with English abstract)
- Chu NC, Taylor RN, Chavagnac V, Nesbitt RW, Boella RM, Milton JA, German CR, Bayon G and Burton K. 2002. Hf isotope ratio analysis using multi-collector inductively coupled plasma mass spectrometry: An evaluation of isobaric interference corrections. *Journal of Analytical Atomic Spectrometry*, 17(12): 1567~1574
- Coleman RG and Peterman ZE. 1975. Oceanic plagiogranite. *Journal of Geophysical Research*, 80(8): 1099~1108
- Coleman RG and Donato MM. 1979. Oceanic plagiogranite revisited. In: Barker F (ed.). *Trondhjemites, Dacites, and Related Rocks*. Amsterdam: Elsevier, 149~167
- Corfu F and Stott GM. 1993. Age and petrogenesis of two Late Archean magmatic suites, northwestern Superior Province, Canada: Zircon U-

- Pb and Lu-Hf isotopic relations. *Journal of Petrology*, 34(4): 817–838
- Ding X, Sun WD, Wang FY, Chen LL, Li QL and Chen FK. 2012. Single-grain mica Rb-Sr isochron ages and mineral chemistry for the Weishan pluton in Hunan Province and implications on petrogenesis and mineralization of Mesozoic composite granite in South China. *Acta Petrologica Sinica*, 28(12): 3823–3840 (in Chinese with English abstract)
- Ding X, Hu YH, Zhang H, Li CY, Ling MX and Sun WD. 2013. Major Nb/Ta fractionation recorded in garnet amphibolite facies metagabbro. *The Journal of Geology*, 121(3): 255–274
- Feng ZS, Zhang ZC, Li JF and Guo ZJ. 2010. Geochemistry and geological significance of the Cretaceous OIB-type mafic dykes in Sanweishan, Dunhuang, Gansu Province. *Acta Petrologica Sinica*, 26(2): 607–616 (in Chinese with English abstract)
- Flagler PA and Spray JG. 1991. Generation of plagiogranite by amphibolite anatexis in oceanic shear zones. *Geology*, 19(1): 70–73
- France L, Koepke J, Ildefonse B, Cichy SB and Deschamps F. 2010. Hydrous partial melting in the sheeted dike complex at fast spreading ridges: Experimental and natural observations. *Contributions to Mineralogy and Petrology*, 160(5): 683–704
- Gao J, Long LL, Qian Q, Huang DZ, Su W and Klemd R. 2006. South Tianshan: A Late Paleozoic or a Triassic orogen? *Acta Petrologica Sinica*, 22(5): 1049–1061 (in Chinese with English abstract)
- Ge RF, Zhu WB, Wu HL, Zheng BH, Zhu XQ and He JW. 2012. The Paleozoic northern margin of the Tarim Craton: Passive or active? *Lithos*, 142–143: 1–15
- Gerlach DC, Leaman WP and Lallemand HGA. 1981. Petrology and geochemistry of plagiogranite in the Canyon Mountain ophiolite, Oregon. *Contributions to Mineralogy and Petrology*, 77(1): 82–92
- Griffin WL, Pearson NJ, Belousova E, Jackson SE, Achterbergh EV, O'Reilly SY and Shee SR. 2000. The Hf isotope composition of cratonic mantle: LAM-MC-ICPMS analysis of zircon megacrysts in kimberlites. *Geochimica et Cosmochimica Acta*, 64(1): 133–147
- Griffin WL, Wang X, Jackson SE, Pearson NJ, O'Reilly SY, Xu XS and Zhou XM. 2002. Zircon chemistry and magma mixing, SE China: In-situ analysis of Hf isotopes, Tonglu and Pingtan igneous complexes. *Lithos*, 61(3–4): 237–269
- He ZY, Zhang ZM, Zong KQ, Xiang H and Klemd R. 2014. Metamorphic  $P-T-t$  evolution of mafic HP granulites in the northeastern segment of the Tarim Craton (Dunhuang block): Evidence for Early Paleozoic continental subduction. *Lithos*, 196–197: 1–13
- Jafri SH, Charan SN and Govil PK. 1995. Plagiogranite from the Andaman ophiolite belt, Bay of Bengal, India. *Journal of the Geological Society*, 152(4): 681–687
- Jahn BM, Wu FY and Chen B. 2000. Granitoids of the Central Asian Orogenic Belt and continental growth in the Phanerozoic. *Transactions of the Royal Society of Edinburgh: Earth Sciences*, 91(1–2): 181–193
- Jian P, Liu DY and Sun XM. 2003a. SHRIMP dating of Carboniferous Jinshajiang ophiolite in western Yunnan and Sichuan: Geochronological constraints on the evolution of the Paleo-Tethys oceanic crust. *Acta Geologica Sinica*, 77(2): 217–228 (in Chinese with English abstract)
- Jian P, Liu DY, Zhang Q, Zhang FQ, Shi YR, Shi GH, Zhang LQ and Tao H. 2003b. SHRIMP dating of ophiolite and leucocratic rocks within ophiolite. *Earth Science Frontiers*, 10(4): 439–456 (in Chinese with English abstract)
- Jian P, Liu DY, Kröner A, Windley BF, Shi YR, Zhang FQ, Shi GH, Miao LC, Zhang W, Zhang Q, Zhang LQ and Ren JS. 2008. Time scale of an Early to Mid-Paleozoic orogenic cycle of the long-lived Central Asian Orogenic Belt, Inner Mongolia of China: Implications for continental growth. *Lithos*, 101(3–4): 233–259
- Khain EV, Bibikova EV, Salnikova EB, Kröner A, Gibbscher AS, Didenko AN, Degtyarev KE and Fedotova AA. 2003. The Palaeo-Asian ocean in the Neoproterozoic and Early Palaeozoic: New geochronologic data and palaeotectonic reconstructions. *Precambrian Research*, 122(1–4): 329–358
- Kinny PD and Maas R. 2003. Lu-Hf and Sm-Nd isotope systems in zircon. *Reviews in Mineralogy and Geochemistry*, 53(1): 327–341
- Kovalenko VI, Yarmolyuk VV, Kovach VP, Kotov AB, Kozakov IK, Salnikova EB and Larin AM. 2004. Isotope provinces, mechanisms of generation and sources of the continental crust in the Central Asian mobile belt: Geological and isotopic evidence. *Journal of Asian Earth Sciences*, 23(5): 605–627
- Kozakov IK, Kotov AB, Salnikova EB, Kovach VP, Nataman A, Bibikova EV, Kimozova TI, Todt W, Kröner A, Yakovleva SZ, Lebedeva VI and Sugorakova AM. 2001. Timing of the structural evolution of metamorphic rocks in the Tuva-Mongolian Massif. *Geotectonics*, 35(3): 165–184
- Kröner A, Hegner E, Lehmann B, Heinhorst J, Wingate MTD, Liu DY and Ermelov P. 2008. Palaeozoic arc magmatism in the Central Asian Orogenic Belt of Kazakhstan: SHRIMP zircon ages and whole-rock Nd isotopic systematics. *Journal of Asian Earth Sciences*, 32(2–4): 118–130
- Li JY, Wang KZ, Li YP, Sun GH, Chu CH, Li LQ and Zhu ZX. 2006. Geomorphological features, crustal composition and geological evolution of the Tianshan Mountains. *Geological Bulletin of China*, 25(8): 895–909 (in Chinese with English abstract)
- Li WX and Li XH. 2003. Adakitic granites within the NE Jiangxi ophiolites, South China: Geochemical and Nd isotopic evidence. *Precambrian Research*, 122(1–4): 29–44
- Li WX and Li XH. 2003. Rock types and tectonic significance of the granitoid rocks within ophiolites. *Advance in Earth Sciences*, 18(3): 392–397 (in Chinese with English abstract)
- Liu XC, Chen BL, Jahn BM, Wu GG and Liu YS. 2011. Early Paleozoic (ca. 465 Ma) eclogites from Beishan (NW China) and their bearing on the tectonic evolution of the southern Central Asian Orogenic Belt. *Journal of Asian Earth Sciences*, 42(4): 715–731
- Liu YS, Yu HF, Xin HT, Lu SN, Xie QY and Li Q. 2009. Tectonic units division and Precambrian significant geological events in Altyn Tagh Mountain, China. *Geological Bulletin of China*, 28(10): 1430–1438 (in Chinese with English abstract)
- Long LL, Gao J, Klemd R, Beier C, Qian Q, Zhang X, Wang JB and Jiang T. 2011. Geochemical and geochronological studies of granitoid rocks from the Western Tianshan Orogen: Implications for continental growth in the southwestern Central Asian Orogenic Belt. *Lithos*, 126(3–4): 321–340
- Lu SN, Li HK, Zhang CL and Niu GH. 2008. Geological and geochronological evidence for the Precambrian evolution of the Tarim Craton and surrounding continental fragments. *Precambrian Research*, 160(1–2): 94–107
- Ludwig KR. 2003. ISOPLOT 3.0: A geochronological toolkit for Microsoft Excel. Berkeley Geochronology Center, Special Publication No. 4
- Ma XX, Shu LS, Meert JG and Li JY. 2014. The Paleozoic evolution of Central Tianshan: Geochemical and geochronological evidence. *Gondwana Research*, 25(2): 797–819
- Mei HL, Yu HF and Li Q. 1997. Preliminary litho-tectonic framework of Early Precambrian rocks in Dunhuang-Beishan area, Gansu, west China. *Progress in Precambrian Research*, 20(4): 47–54 (in Chinese with English abstract)
- Mei HL, Yu HF, Lu SN, Li HM, Li Q, Lin YX and Zuo YC. 1998. Archean tonalite in the Dunhuang, Gansu Province: Age from the U-Pb single zircon and Nd isotope. *Progress in Precambrian Research*, 21(1): 41–45 (in Chinese with English abstract)
- Meng FC, Zhang JX, Xiang ZQ, Yu SY and Li JP. 2011. Evolution and formation of the Dunhuang Group in NE Tarim basin, NW China: Evidence from detrital-zircon geochronology and Hf isotope. *Acta Petrologica Sinica*, 27(1): 59–76 (in Chinese with English abstract)
- Mojzsis SJ and Harrison TM. 2002. Establishment of a 3.83-Ga magmatic age for the Akilia tonalite (southern West Greenland). *Earth and Planetary Science Letters*, 202(3–4): 563–576

- Patchett PJ, Kouvo O, Hedge CE and Tasomoto M. 1982. Evolution of continental crust and mantle heterogeneity: Evidence from Hf isotopes. *Contributions to Mineralogy and Petrology*, 78 (3): 279–297
- Pearce JA. 1989. High T/P metamorphism and granite genesis beneath ophiolite thrust sheets. *Ophioliti*, 14(3): 195–211
- Pedersen RB and Malpas J. 1984. The origin of oceanic plagiogranites from the Karmoy ophiolite, western Norway. *Contributions to Mineralogy and Petrology*, 88(1–2): 36–52
- Peters T and Kamber BS. 1994. Peraluminous, potassium-rich granitoids in the Semail ophiolite. *Contributions to Mineralogy and Petrology*, 118(3): 229–238
- Qu JF, Xiao WJ, Windley BF, Han CM, Mao QG, Ao SJ and Zhang JE. 2011. Ordovician eclogites from the Chinese Beishan: Implications for the tectonic evolution of the southern Altaids. *Journal of Metamorphic Geology*, 29(8): 803–820
- Rowley DB, Xue F, Tucker RD, Peng ZX, Baker J and Davis A. 1997. Ages of ultrahigh pressure metamorphism and protolith orthogneisses from the eastern Dabie Shan: U/Th zircon geochronology. *Earth and Planetary Science Letters*, 151(3–4): 191–203
- Rubatto D and Gebauer D. 2000. Use of cathodoluminescence for U-Pb zircon dating by IOM Microprobe: Some examples from the western Alps. In: *Cathodoluminescence Geoscience*. Berlin Heidelberg: Springer-Verlag, 373–400
- Rudnick RL and Gao S. 2003. Composition of the continental crust. In: Heinrich DH and Karl KT (eds.). *Treatise on Geochemistry*. Oxford: Pergamon, 1–64
- Scarow JH, Pease V, Fleutelot C and Dushin V. 2001. The Late Neoproterozoic Enganepe ophiolite, Polar Urals, Russia: An extension of the Cadomian arc? *Precambrian Research*, 110(1–4): 255–275
- Searle MP and Malpas J. 1980. Structure and metamorphism of rocks beneath the Semail ophiolite of Oman and their significance in ophiolite obduction. *Transactions of the Royal Society of Edinburgh: Earth Sciences*, 71(4): 247–262
- Sengör AMC and Natal'ın BA. 1993. Turkic-type orogeny in the Altaids: Implications for the evolution of continental crust and methodology of regional tectonic analysis. *Transactions of the Leicester Literary & Philosophical Society*, 87: 37–47
- Sengör AMC, Natal'ın BA and Burtman VS. 1993. Evolution of the Altai tectonic collage and Palaeozoic crustal growth in Eurasia. *Nature*, 364(6435): 299–307
- Shi YR, Liu DY, Zhang Q, Jian P, Zhang FQ and Miao LC. 2007. SHRIMP zircon U-Pb dating of the Gangou granitoids, Central Tianshan Mountains, Northwest China and tectonic significances. *Chinese Science Bulletin*, 52(11): 1507–1516
- Su CQ, Jiang CY, Xia MZ, Wei W and Pan R. 2009. Geochemistry and zircons SHRIMP U-Pb age of volcanic rocks of Aqishan Formation in the eastern area of North Tianshan, China. *Acta Petrologica Sinica*, 25(4): 901–915 (in Chinese with English abstract)
- Sun SS and McDonough WF. 1989. Chemical and isotopic systematics of ocean basalts: Implication for mantle composition and processes. In: Saunders AD and Norry MJ (eds.). *Magmatism in the Ocean Basins*. Geological Society, London, Special Publications, 42(1): 313–345
- Sun WD, Williams IS and Li SG. 2002. Carboniferous and Triassic eclogites in the western Dabie Mountains, east-central China: Evidence for protracted convergence of the North and South China Blocks. *Journal of Metamorphic Geology*, 20(9): 873–886
- Sun Y, Che ZC, Liu CY, Zhang XH, Shen WH and Fu XF. 1992. Composition and tectonic characteristics of the Archean Altun basement complex. *Journal of Northwest University*, 22(S1): 101–114 (in Chinese with English abstract)
- Wang X. 1993. Characteristics of zircon in plagiogranite from Inzecca, France and its geological significance. *Chinese Science Bulletin*, 38(6): 534–537 (in Chinese)
- Whitehead J, Dunning GR and Spray JG. 2000. U-Pb geochronology and origin of granitoid rocks in the Thetford Mines ophiolite, Canadian Appalachians. *Geological Society of America Bulletin*, 112(6): 915–928
- Windley BF, Badarch G, Cunningham WD, Kröner A, Buchan AC, Tomurtogoo O and Salnikova EB. 2001. Subduction-accretion history of the Central Asian Orogenic Belt: Constraints from Mongolia. *Gondwana Research*, 4(4): 825–826
- Windley BF, Alexeev D, Xiao WJ, Kröner A and Badarch G. 2007. Tectonic models for accretion of the Central Asian Orogenic Belt. *Journal of the Geological Society*, 164(1): 31–47
- Wu FY, Li XH, Zheng YF and Gao S. 2007. Lu-Hf isotopic systematics and their applications in petrology. *Acta Petrologica Sinica*, 23(2): 185–220 (in Chinese with English abstract)
- Xia B, Zhang LF, Xia Y and Thomas B. 2014. The tectonic evolution of the Tianshan orogenic belt: Evidence from U-Pb dating of detrital zircons from the Chinese southwestern Tianshan accretionary mélange. *Gondwana Research*, 25(4): 1627–1643
- Xiao WJ, Huang BC, Han CM, Sun S and Li JL. 2010. A review of the western part of the Altaids: A key to understanding the architecture of accretionary orogens. *Gondwana Research*, 18(2–3): 253–273
- Xiao WJ, Windley BF, Allen MB and Han CM. 2013. Paleozoic multiple accretionary and collisional tectonics of the Chinese Tianshan orogenic collage. *Gondwana Research*, 23(4): 1316–1341
- Xiao WJ and Santosh M. 2014. The western Central Asian Orogenic Belt: A window to accretionary orogenesis and continental growth. *Gondwana Research*, 25(4): 1429–1444
- Xin HT, Liu YS, Luo ZH, Song SC and Wang SQ. 2013. The growth of Archean continental crust in Aqtashtagh area of Southeast Tarim, China: Constraints from petrochemistry and chronology about Milan Group and TTG gneiss. *Earth Science Frontiers*, 20(1): 240–259 (in Chinese with English abstract)
- Xu ZQ, Yang JS, Zhang JX, Jiang M, Li HB and Cui JW. 1999. A comparison between the tectonic units on the two sides of the mechanism of lithospheric shearing. *Acta Geologica Sinica*, 73(3): 193–205 (in Chinese with English abstract)
- Zhang JX, Li HK, Meng FC, Xiang ZQ, Yu SY and Li JP. 2011. Polyphase tectono-thermal events recorded in “metamorphic basement” from the Altyn Tagh, the southeastern margin of the Tarim basin, western China: Constraint from U-Pb zircon geochronology. *Acta Petrologica Sinica*, 27(1): 23–46 (in Chinese with English abstract)
- Zhang JX, Gong JH and Yu SY. 2012. Ca. 1.85 Ga HP granulite-facies metamorphism in the Dunhuang block of the Tarim Craton, NW China: Evidence from U-Pb zircon dating of mafic granulites. *Journal of the Geological Society*, 169(5): 511–514
- Zhang JX, Yu SY, Gong JH, Li HK and Hou KJ. 2013. The latest Neoarchean-Paleoproterozoic evolution of the Dunhuang block, eastern Tarim craton, northwestern China: Evidence from zircon U-Pb dating and Hf isotopic analyses. *Precambrian Research*, 226(1): 21–42
- Zhang LC, Qin KZ, Ying JF, Xia B and Shu JS. 2004. The relationship between ore-forming processes and adakitic rock in Tuwu-Yandong porphyry copper metallogenic belt, eastern Tianshan Mountains. *Acta Petrologica Sinica*, 20(2): 259–268 (in Chinese with English abstract)
- Zhang Q, Wang Y, Xiong XL and Li CD. 2008. Adakite and Granite: Challenge and Opportunity. Beijing: China Land Press, 29–30 (in Chinese with English abstract)
- Zhang ZC, Guo ZJ, Zou GQ, Feng ZS and Li JF. 2009. Geochemical characteristics and SHRIMP U-Pb age of zircons from the Danghe reservoir TTG in Dunhuang, Gansu Province, and its significations. *Acta Petrologica Sinica*, 25(3): 495–505 (in Chinese with English abstract)
- Zhao Y, Diwu CR, Sun Y, Zhu T and Wang HL. 2013. Zircon geochronology and Lu-Hf isotope compositions for Precambrian rocks of the Dunhuang complex in Shuixiakou area, Gansu Province. *Acta Petrologica Sinica*, 29(5): 1698–1712 (in Chinese with English abstract)
- Zhao Y, Diwu CR, Ao WH, Wang HL, Zhu T and Sun Y. 2015. Ca.

- 3.06 Ga granodioritic gneiss in Dunhuang block. Chinese Science Bulletin, 60(1): 75–87 (in Chinese)
- Zheng RG, Wu TR, Zhang W, Feng JC, Xu C, Meng QP and Zhang ZY. 2013. Geochronology and geochemistry of the Yagan granite in the northern margin of the Alxa block: Constraints on the tectonic evolution of the southern Altaids. Acta Petrologica Sinica, 29(8): 2665–2675 (in Chinese with English abstract)
- Zheng RG, Wu TR, Zhang W, Xu C, Meng QP and Zhang ZY. 2014. Late Paleozoic subduction system in the northern margin of the Alxa block, Altaids: Geochronological and geochemical evidence from ophiolites. Gondwana Research, 25(2): 842–858
- Zhou TF, Yuan F, Zhang DY, Fan Y, Liu S, Peng MX and Zhang JD. 2010. Geochronology, tectonic setting and mineralization of granitoids in Jueluotage area, eastern Tianshan, Xinjiang. Acta Petrologica Sinica, 26(2): 478–502 (in Chinese with English abstract)
- Zhu T, Wang HL, Xu XY, Chen JL, Ma ZP, Li ZP, Zhu XH and Li P. 2014. Discovery of adakitic rocks in south margin of Dunhuang block and its geological significance. Acta Petrologica Sinica, 30(2): 491–502 (in Chinese with English abstract)
- Zong KQ, Zhang ZM, He ZY, Hu ZC, Santosh M, Liu YS and Wang W. 2012. Early Palaeozoic high-pressure granulites from the Dunhuang block, northeastern Tarim Craton: Constraints on continental collision in the southern Central Asian Orogenic Belt. Journal of Metamorphic Geology, 30(8): 753–768
- Zong KQ, Liu YS, Zhang ZM, He ZY, Hu ZC, Guo JL and Chen K. 2013. The generation and evolution of Archean continental crust in the Dunhuang block, northeastern Tarim Craton, northwestern China. Precambrian Research, 235: 251–263
- 梅华林, 于海峰, 李铨. 1997. 甘肃敦煌-北山早前寒武纪岩石组合-构造初步框架. 前寒武纪研究进展, 20(4): 47–54
- 梅华林, 于海峰, 陆松年, 李惠民, 李铨, 林源贤, 左义成. 1998. 甘肃敦煌太古宙英云闪长岩: 单颗粒锆石 U-Pb 年龄和 Nd 同位素. 前寒武纪研究进展, 21(1): 41–45
- 孟繁聪, 张建新, 相振群, 于胜尧, 李金平. 2011. 塔里木盆地东北缘敦煌群的形成和演化: 锆石 U-Pb 年代学和 Lu-Hf 同位素证据. 岩石学报, 27(1): 59–76
- 苏春乾, 姜常义, 夏明哲, 魏巍, 潘荣. 2009. 北天山东段阿奇山组火山岩的地球化学特征及锆石 U-Pb 年龄. 岩石学报, 25(4): 901–915
- 孙勇, 车自成, 刘池阳, 张晓会, 沈卫宏, 付晓风. 1992. 阿尔金山隆起区下地壳断块的组成和构造意义. 西北大学学报, 22(增刊): 101–114
- 汪相. 1993. 法国 Inzecca 斜长花岗岩中的锆石特征及其地质意义. 科学通报, 38(6): 534–537
- 吴福元, 李献华, 郑永飞, 高山. 2007. Lu-Hf 同位素体系及其岩石学应用. 岩石学报, 23(2): 185–220
- 辛后田, 刘永顺, 罗照华, 宋顺昌, 王树庆. 2013. 塔里木盆地东南缘阿克塔什塔格地区新太古代陆壳增生: 米兰岩群和 TTG 片麻岩的地球化学及年代学约束. 地学前缘, 20(1): 240–259
- 许志琴, 杨经绥, 张建新, 姜枚, 李海兵, 崔军文. 1999. 阿尔金断裂两侧构造单元的对比及岩石圈剪切机制. 地质学报, 73(3): 193–205
- 张建新, 李怀坤, 孟繁聪, 相振群, 于胜尧, 李金平. 2011. 塔里木盆地东南缘(阿尔金山)“变质基底”记录的多期构造热事件: 锆石 U-Pb 年代学的制约. 岩石学报, 27(1): 23–46
- 张连昌, 秦克章, 英基丰, 夏斌, 舒建生. 2004. 东天山土屋-延东斑岩铜矿带埃达克岩及其与成矿作用的关系. 岩石学报, 20(2): 259–268
- 张旗, 王焰, 熊小林, 李承东. 2008. 埃达克岩和花岗岩: 机遇与挑战. 北京: 中国大地出版社, 29–30
- 张志诚, 郭召杰, 邹冠群, 冯志硕, 李建锋. 2009. 甘肃敦煌党河水系 TTG 地球化学特征、锆石 SHRIMP U-Pb 定年及其构造意义. 岩石学报, 25(3): 495–505
- 赵燕, 第五春荣, 孙勇, 朱涛, 王洪亮. 2013. 甘肃敦煌水峡口地区前寒武纪岩石的锆石 U-Pb 年龄、Hf 同位素组成及其地质意义. 岩石学报, 29(5): 1698–1712
- 赵燕, 第五春荣, 敖文昊, 王洪亮, 朱涛, 孙勇. 2015. 敦煌地块发现 ~3.06 Ga 花岗闪长质麻岩. 科学通报, 60(1): 75–87
- 郑国国, 吴泰然, 张文, 冯继承, 徐操, 孟庆鹏, 张昭昱. 2013. 阿拉善地块北缘雅干花岗岩体地球化学、地质年代学及其对区域构造演化制约. 岩石学报, 29(8): 2665–2675
- 周涛发, 袁峰, 张达玉, 范裕, 刘帅, 彭明兴, 张建滇. 2010. 新疆东天山觉罗塔格地区花岗岩类年代学、构造背景及其成矿作用研究. 岩石学报, 26(2): 478–502
- 朱涛, 王洪亮, 徐学义, 陈隽璐, 马中平, 李智佩, 朱小辉, 李平. 2014. 敦煌地块南缘石炭纪埃达克岩的发现及其地质意义. 岩石学报, 30(2): 491–402

## 附中文参考文献

- 陈刚, 朱志新, 董连慧, 刘斌, 倪新元, 赵恒乐. 2010. 新疆南天山塔什库尔干泥盆-早石炭世洋岛型火山岩的确定及地质意义. 新疆地质, 28(3): 236–241
- 陈岳龙, 李大鹏, 刘长征, 王忠, 刘金宝. 2013. 中亚造山带的形成与演化历史: 来自锆石 U-Pb 年龄与 Hf 同位素及全岩 Nd 同位素组成的证据. 地质学报, 87(增刊): 374–376
- 丁兴, 孙卫东, 汪方跃, 陈林丽, 李秋立, 陈福坤. 2012. 湖南沩山岩体多期云母的 Rb-Sr 同位素年龄和矿物化学组成及其成岩成矿指示意义. 岩石学报, 28(12): 3823–3840
- 冯志硕, 张志诚, 李建锋, 郭召杰. 2010. 敦煌三危山地区白垩纪 OIB 型基性岩墙的特征及其地质意义. 岩石学报, 26(2): 607–616
- 高俊, 龙灵利, 钱青, 黄德志, 苏文, Klemd R. 2006. 南天山: 晚古生代还是三叠纪碰撞造山带? 岩石学报, 22(5): 1049–1061
- 简平, 刘敦一, 孙晓猛. 2003a. 滇川西部金沙江石炭纪蛇绿岩 SHRIMP 测年: 古特提斯洋壳演化的同位素年代学制约. 地质学报, 77(2): 217–228
- 简平, 刘敦一, 张旗, 张福勤, 石玉若, 施光海, 张履桥, 陶华. 2003b. 蛇绿岩及蛇绿岩中浅色岩的 SHRIMP U-Pb 测年. 地学前缘, 10(4): 439–456
- 李锦铁, 王克卓, 李亚萍, 孙桂华, 褚春华, 李丽群, 朱志新. 2006. 天山山脉地貌特征、地壳组成与地质演化. 地质通报, 25(8): 895–909
- 李武显, 李献华. 2003. 蛇绿岩中的花岗质岩石成因类型与构造意义. 地球科学进展, 18(3): 392–397
- 刘永顺, 于海峰, 辛后田, 陆松年, 修群业, 李铨. 2009. 阿尔金山地区构造单元划分和前寒武纪重要地质事件. 地质通报, 28